

X-ray Studies and Magnetic Ordering Modeling of Chains of Magnetite Nanoparticles

Dallin Smith

A senior thesis submitted to the faculty of
Brigham Young University
in partial fulfillment of the requirements for the degree of

Bachelor of Science

Karine Chesnel, Advisor

Department of Physics and Astronomy

Brigham Young University

April 2016

Copyright © 2016 Dallin Smith

All Rights Reserved

ABSTRACT

X-ray Studies and Magnetic Ordering Modeling of Chains of Magnetite Nanoparticles

Dallin Smith

Department of Physics and Astronomy, BYU

Bachelor of Science

The study of magnetic nanoparticles has attracted attention for biomedical and nanotechnology research. Magnetite Fe_3O_4 is a ferrimagnetic nanoparticle carrying a macro-magnetic spin. When the nanoparticles self-assemble on a membrane, they interact with each other and demonstrate a superparamagnetic behavior. To understand these properties, we use several x-ray techniques: x-ray absorption spectroscopy (XAS), x-ray magnetic circular dichroism (XMCD) and x-ray magnetic resonant scattering (XRMS). With these procedures we can study the electronic structure and obtain a magnetic profile for the nanoparticles. Having acquired such data at the SLAC synchrotron, we examined different nanoparticles sizes and concentrations, at different x-ray energies and various temperatures and under the application of different magnetic field strengths. Models were made to fit the experimental data to outline the physical structure and the magnetic order from the XMCD and XRMS experiments. More importantly, the modeling concluded about the magnetic order of the specific magnetic spin configuration of the nanoparticle assembly, under the application of a given magnetic field at a given temperature.

Keywords: Magnetite (Fe_3O_4), Superparamagnetism, Magnetic Order, Dichroic Effect, Modeling

ACKNOWLEDGMENTS

I would like to express my profound appreciation to Dr. Karine Chesnel for her contributions. She has spent numerous hours training and guiding me through this research experience. She has been an outstanding mentor and teacher. Her unfailing desire to help me has given me many opportunities to learn and grow in the physics realm. I would also like to thank the Brigham Young University's Physics and Astronomy department in financially supporting me as a research assistant and scholarships. I want to thank Stanford Synchrotron Radiation Lightsource (SSRL) for allowing my research group to use their facilities. Finally, I would like to thank my family and friends in supporting me this research project. My mother for her unwavering confidence in me and my father for assisting me in various academic projects. In all, I want to express gratitude for everyone that has assisted me in any way.

Contents

Table of Contents	iv
List of Figures	v
1 Introduction	1
1.1 Background	1
1.2 Fabrication	2
1.3 Magnetic Behavior of Magnetite Nanoparticles	3
2 Synchrotron X-ray Studies	6
2.1 Synchrotron Setup	6
2.2 X-ray Absorption Spectroscopy (XAS)	7
2.3 X-ray Magnetic Circular Dichroism (XMCD)	9
2.4 X-ray Resonant Magnetic Scattering (XRMS)	11
2.5 Finding the Distance to Detector	13
2.6 XRMS Profiles	15
2.7 Dichroic Signal	17
2.8 Conclusion	20
3 Structural Modeling of the Nanoparticle Chain	21
3.1 Introduction	21
3.2 Charge Density Function	22
3.3 Nanoparticle Size Distribution	23
3.4 Scattering Intensity	25
3.5 Results of Model Fits	26
3.6 Temperature Dependence Study	29
4 Modeling of the Magnetic Ordering	31
4.1 Magnetic Spin Function	31
4.2 Setting Constraints	34
4.3 Magnetic Spin Function Results	36

Appendix A	XRMS Analyzing Program	41
A.1	Converting SPE and DAT	44
A.2	Making Ring Set and Blocker	44
A.3	Generating Profiles	46
A.4	Extracting Dichroic Signals	48
Appendix B	Graphs of Model Fits	50
Bibliography		55
Index		56

List of Figures

1.1	Our Three Nanoparticles batches: NP16, NP17, NP18	3
1.2	Illustration Of Superparamagnetism	4
2.1	Vacuum Chamber	7
2.2	XAS diagram	8
2.3	X-ray Absorption Spectrum	9
2.4	X-ray Magnetic Circular Dichroism Plot	10
2.5	X-ray Resonant Magnetic Scattering Diagram	11
2.6	XRMS Image and profile	12
2.7	Diagram of Finding D	14
2.8	Dichroic Effect Plots	18
2.9	Magnetization Loop	19
3.1	Sketch of Nanoparticle Chain	22
3.2	The Charge Density Function	23
3.3	The Distribution of NP	24
3.4	The Fourier Transform of the Charge Density Function	26
3.5	Models Of The XRMS Profile	27
3.6	Modeling the effect of Temperature	30

4.1	Magnetization Loop	32
4.2	Diagram of Magnetic Ordering	33
4.3	The Magnetic Spin Function	34
4.4	Vibrating Sample Magnetometer	35
4.5	Plots of Magnetic Order Coefficients	37
4.6	Models of the Magnetic Ratio	38
A.1	XRMS Analyzing Program	42
A.2	Folder Directory	43
A.3	Ring Set and Blocker	45
A.4	Angular Integration	48
B.1	Models Of The XRMS Profile Part 1	51
B.2	Models Of The XRMS Profile Part 2	52
B.3	Models of the Magnetic Ratio for Sample 2	53
B.4	Models of the Magnetic Ratio for Sample 3	54

Chapter 1

Introduction

1.1 Background

Nanotechnology is playing an important role in today's world. Its applications are endless and they continue to improve our living conditions around the world. Magnetite (Fe_3O_4) nanoparticles have the capacity to be instrumental in various biomedical treatments such as magnetic resonance imaging (MRI) techniques, drug delivery, specifically cancer magnetic nanotherapy, and magnetic hyperthermia. (Akbarzadeh et al. 2012) Magnetite is non-toxic to humans and can flow in the blood stream for operative purposes. (Ito et al. 2005)

We want to measure the magnetic behavior of Fe_3O_4 nanoparticles when assembled on a membrane for different nanoparticle sizes. We fabricated various samples of different nanoparticles sizes and used a transmission electron microscopy (TEM) to study the size and concentration of the nanoparticle assembly in each batch. We want to know if the structure of the nanoparticle samples influences its magnetic order. As the nanoparticles interact with each other, they produce the magnetic effect called superparamagnetism. (Bean & Livingston 1959) We used various techniques to study our magnetite nanoparticles assemblies. Three synchrotron techniques were used

to obtain a magnetic signal and further our understanding of the sample structure. These techniques are: x-ray absorption spectroscopy (XAS), x-ray magnetic circular dichroism (XMCD), and x-ray magnetic resonant scattering (XRMS). Many variables may affect the magnetic ordering, therefore, in the noted experiments, the temperature and external magnetic field were changed giving a large sampling range of data to analyze for comparison. Modeling functions were constructed to compare with the experimental results to bring further knowledge; from it we learned the magnetic behavior and the physical structure of the nanoparticles.

1.2 Fabrication

In collaboration with Dr. Harrison in the Chemistry department of Brigham Young University, we fabricated three different nanoparticle batches: NP16, NP17, and NP18. Three nanoparticles were synthesized using an organic method. The size of the nanoparticles was controlled by the thermal decomposition of an iron precursor. (Sun* et al. 2002) The temperature of the nanoparticle solution was the determining factor of particles sizes. For the smallest nanoparticle (NP18), the solution was set at 260 C, for NP17, it was set at 290 C, and for the largest (NP16) it was set at 320 C. (Cai et al. 2014)

Each of the three different batches of Fe_3O_4 nanoparticles (NP16), (NP17), (NP18) were deposited onto 50 nm Si_3O_4 membrane with various concentrations. With the different concentrations, we produced a set of nine samples. All of the membranes had a window size of 100 x 100 μm . The nanoparticles on the membrane self-assembled a hexagonal lattice. (Cai et al. 2014) The concentration was carefully controlled in an attempt to achieve a monolayer of these nanoparticles. By varying the nanoparticle concentration, we obtained some variance in the interparticle distance. Once deposited on the membrane, images were taken with a transmission electron microscopy (TEM) as shown in Figure 1.1, to assess the average size of the nanoparticles. The results from

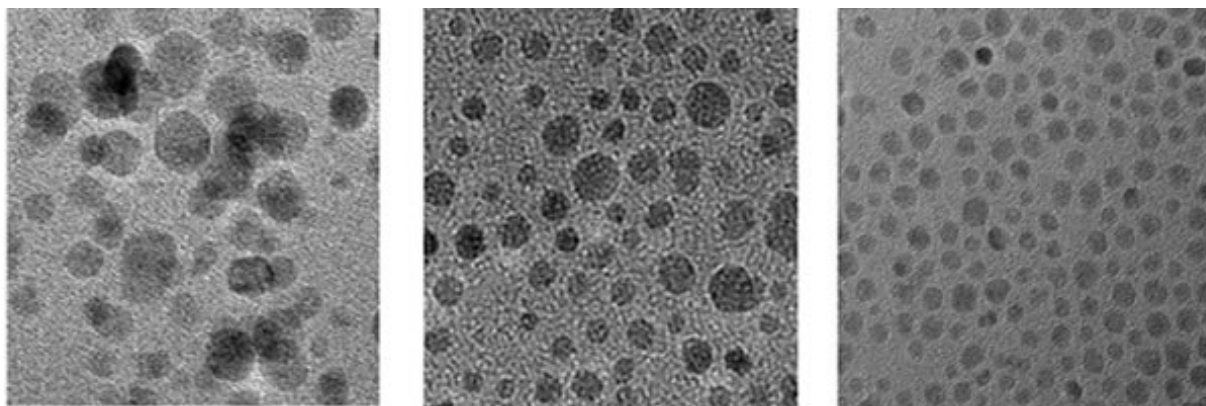


Figure 1.1 Nanoparticles placed on a Si₃N₄ membrane at three different concentrations were used. From the left to right the first picture is NP16 with the average size of 11 nm. The middle image is NP17 with the average size of 8 nm and the right picture is NP18 with the average of 5 nm (Cai et al. 2014)

these measurements gave an estimate of the nanoparticles sizes between 5 and 11 nm, specifically for NP16: 11.3 nm \pm 2.5 nm, for NP17: 8.1 nm \pm 1.7 nm, and for NP18: 5.6 nm \pm 1 nm.

1.3 Magnetic Behavior of Magnetite Nanoparticles

Before we start defining the magnetic behavior of magnetite nanoparticles, several magnetic characteristics need to be defined. Ferromagnetic ordering is the strongest form of magnetism and occurs because the strongly coupled electron spins align parallel with each other. Anti-ferromagnetism occurs when the strongly coupled electrons align antiparallel, thus the net magnetization is zero. In paramagnetism the intrinsic spins are not strongly coupled so they do not align, unless a magnetic field is applied. The individual spins in the material begin to align when an external magnetic field is applied. Ferrimagnetic materials are very similar to antiferromagnetic materials except that the opposing spins are unequal in magnitude and a spontaneous magnetization remains. (Spaldin 2010) Our Fe₃O₄ nanoparticles are ferrimagnetic as they contain three different types of magnetic spins carried by the Fe²⁺ and Fe³⁺ ions. These different magnetic spins were studied in XMCD

experiments and will be further explained in detail in Chapter 2.

The thousands of these Fe^{2+} and Fe^{3+} atomic spins, ordering ferrimagnetically, which comprises these nanoparticles create an overall macro-spin for the individual nanoparticles. As the nanoparticles assemble together on a membrane, the orientation of the macro-spin are oriented in a chaotic manner by pointing in different directions. Thus, in the absence of external field, the overall magnetization of a nanoparticle assembly is close to zero. However, when an external magnetic field is applied to the nanoparticle assembly, the macro-spin of each nanoparticle begins to align with the external field. Depending on the strength of the external magnetic field, more macro-spins tend to align. When all of the macro spins align with the external field, the net magnetization

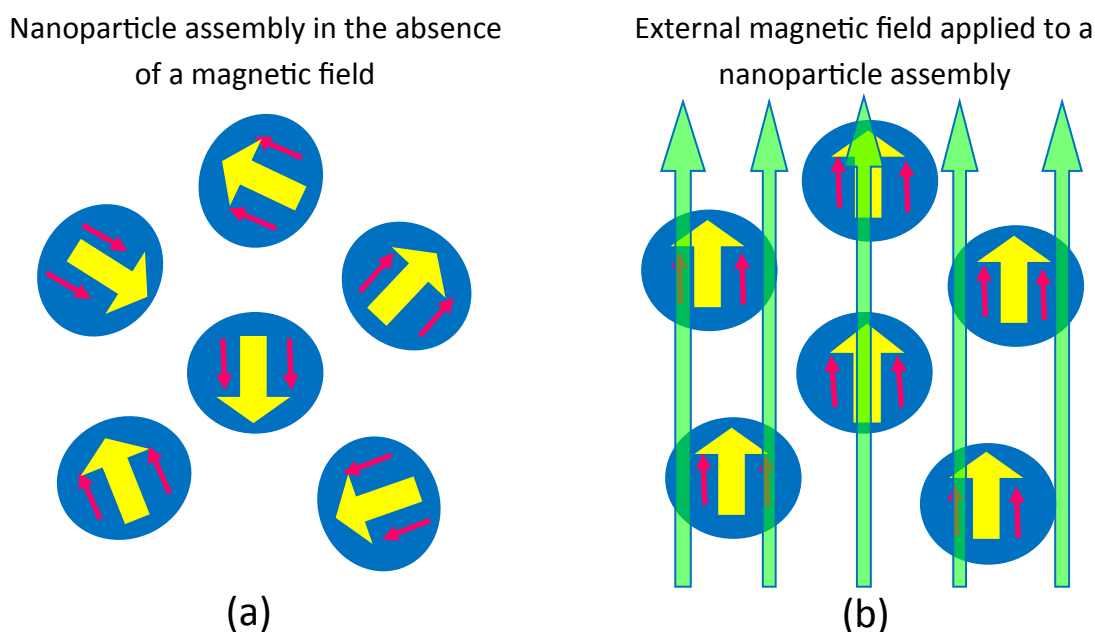


Figure 1.2

a) sketch of a nanoparticle assembly consisting of ferrimagnetic particles, here represented in the absence of a magnetic field. The small one-dimensional arrows are the ferrimagnetic domains exhibited by Fe^3 and Fe^2 of each particle. The overall nanoparticle contains a magnetic moment which is symbolized as the big yellow arrows. (b) phenomenon of superparamagnetism is illustrated as each nanoparticle's magnetic moment is aligned with an external magnetic field thus creating a macro magnetic moment of the entire system.

reaches a maximum called saturation.

This overall behavior, occurring at the nano scale is called superparamagnetism. In Figure 1.2, the illustration demonstrates the phenomenon of superparamagnetism. The superparamagnetic behavior of the nanoparticle assembly was studied in our synchrotron x-ray experiments to find the magnetic ordering in the nanoparticle assembly. Using x-ray absorption spectroscopy (XAS), x-ray magnetic circular dichroism (XMCD), and x-ray magnetic resonant scattering (XRMS) techniques we could extract the magnetic signal of the nanoparticles to give a large sample size of data. Conclusions about the nanoparticles were made possible by the models that were fitted to the experimental data about the nanoparticle sizes and the magnetic ordering.

Chapter 2

Synchrotron X-ray Studies

2.1 Synchrotron Setup

Our x-ray experiments were carried out at Stanford Linear Accelerator Center (SLAC) at the Stanford Synchrotron Radiation Lightsource (SSRL), at beam line 13-3. Soft monochromatic x-rays were finely tuned to perform x-ray absorption spectroscopy (XAS), x-ray magnetic circular dichroism (XMCD), and x-ray magnetic resonant scattering (XRMS) measurements. Through an elliptical polarization undulator (EPU), the x-rays were circular polarized with a degree of polarization of 98 %. A vacuum of 10^{-5} Torr was needed to avoid absorption of x-rays by air. Our membranes were then mounted on a cryogenic sample holder that was placed inside the vacuum chamber.

An electromagnet with copper wiring created a magnetic field and was placed parallel to the direction of the x-ray beam. An extra permanent magnet provided a stronger magnetic field in order for the Fe_3O_4 particles to reach their magnetization saturation. The extra magnetic field produced up to 6.3 kOe. The x-ray beam cross-section had a size of $200 \times 80 \mu\text{m}$, which nearly covered the entire window size of a nanoparticle membrane of $100 \times 100 \mu\text{m}$. Figure 2.1 shows the inside of the vacuum chamber.

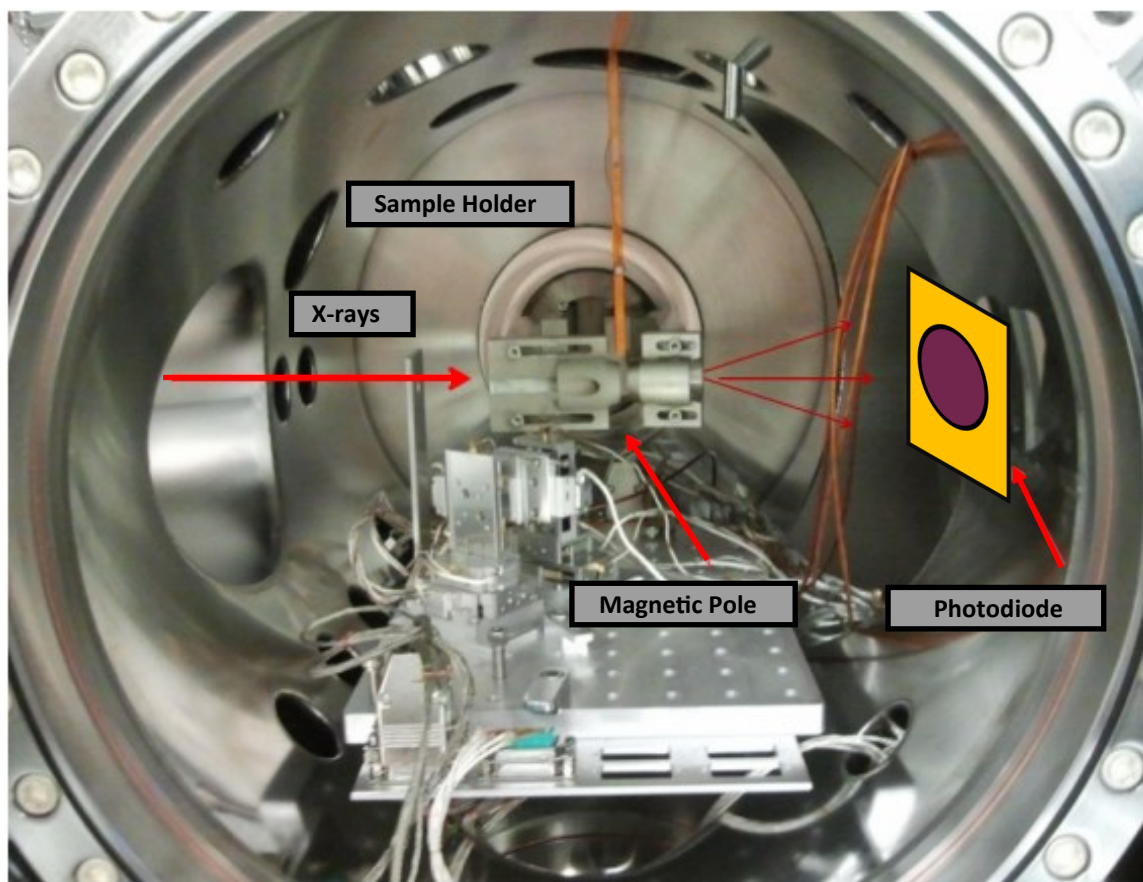


Figure 2.1 Inside of the vacuum scattering chamber. On the left side, the monochromatic x-rays enter the chamber. The sample and external magnetic is placed in the middle of the image on a table. On the right side, a the photodiode and other detectors are placed to capture the transmitted and scattering x-rays.

2.2 X-ray Absorption Spectroscopy (XAS)

X-ray absorption spectroscopy (XAS) is a technique that gives information about the electronic structure of materials. A beam of x-rays illuminates the membrane and passes through the sample window. Downstream of the sample was placed a photodiode to detect the transmitted x-rays through the sample. Figure 2.2 shows a diagram to illustrate the setup to obtain the absorption signal.

The intensity of the transmitted light was recorded as a function of the x-ray energy E . The

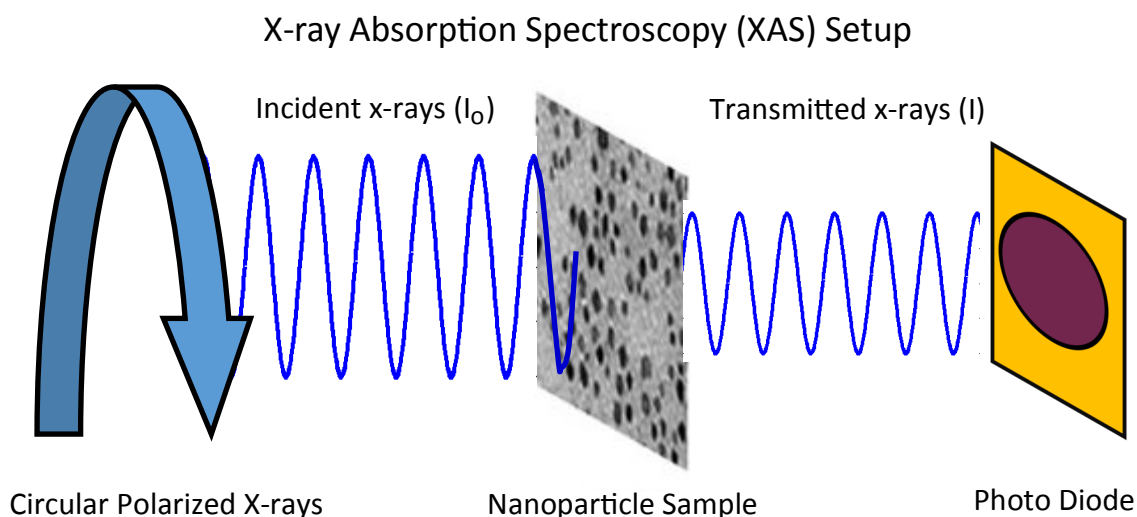


Figure 2.2 This diagram displays the setup used to obtain the x-ray absorption spectrum in the vacuum chamber. Circular polarized x-rays shine onto the nanoparticle sample and the transmitted light is directed towards the photodiode.

range of photon energy E covered 690–735 eV. The energy range was chosen to include the iron $L_{2,3}$ edge, which is at 708 eV. When the photon is at this energy, it excites the dipole transition from the $2p$ state to the $3d$ band. Since Fe_3O_4 contains Fe, a peak in the XAS signal is detected at the resonant frequency. From the transmitted light, we can calculate the absorption intensity. We obtain the XAS signal by normalizing the transmitted signal I by the incoming initial x-rays I_0 . The transmission signal $T = I/I_0$ was converted to an absorption intensity $A = -\ln(T)$ and is displayed in Figure 2.3 .

After acquiring the absorption spectrum, further normalization took place to subtract the background signal. In Figure 2.3, the observed background slope is caused by charge absorption. We use a linear fit to subtract this slope from the spectrum. The subtraction begins at $E = 690$ eV and end just below the first peak at $E = 708$ eV. Another linear fit, was applied from just above the second peak at $E = 720$ eV until the end, at $E = 735$ eV. Afterwards, the gap between low E level and high E level was normalized to the value of one, as shown in Figure 2.4.

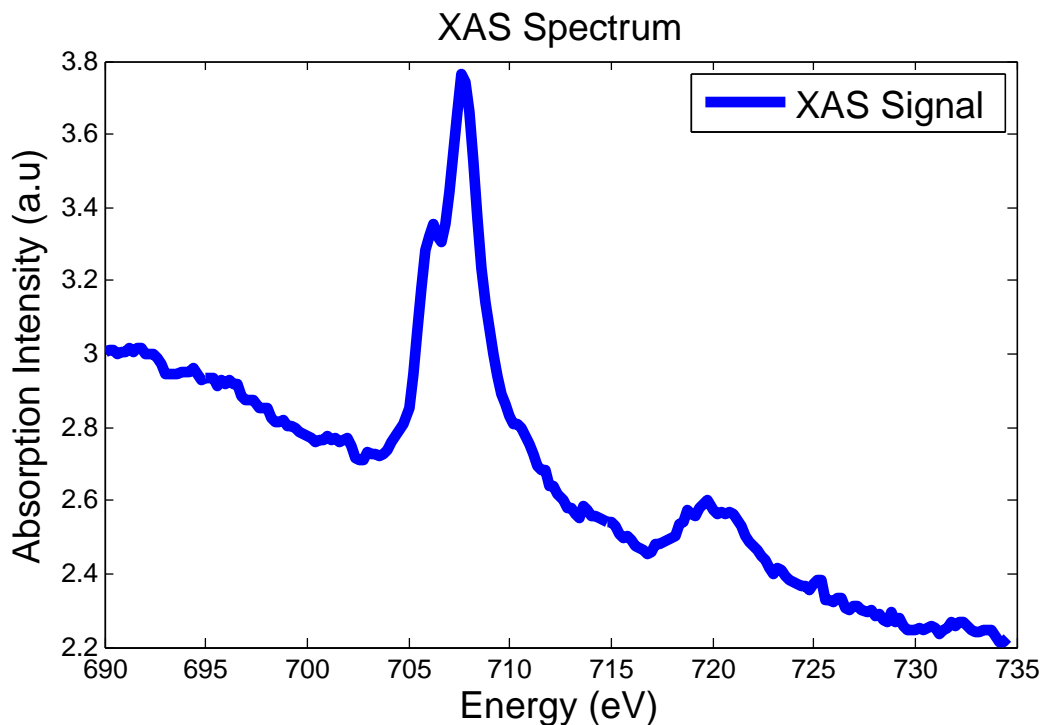


Figure 2.3 XAS spectrum It is a function of intensity versus the energy. We identify the resonant energy of Fe_3O_4 is around 708 eV.

2.3 X-ray Magnetic Circular Dichroism (XMCD)

X-ray magnetic circular dichroism (XMCD) is an extension of XAS. Like in XAS, the photons at the $L_{2,3}$ edge of Fe excites a magnetic resonance material. As the x-rays transfer energy into the system by the angular momentum of the photon, a magnetic transition occurs in the material. Using different helicities of x-rays, namely positive and negative for either left and right circular polarized x-rays, the XMCD is performed by measuring the XAS at opposite helicities. The opposite helicity absorption is plotted in Figure 2.4. An XMCD signal is then extracted by normalizing each of the XAS spectra and taking the difference of those polarized intensity plots. This procedure gives access to magnetic signal. XMCD is an essential tool for measuring the spin and orbital magnetic moments of magnetite. (Cai et al. 2014)

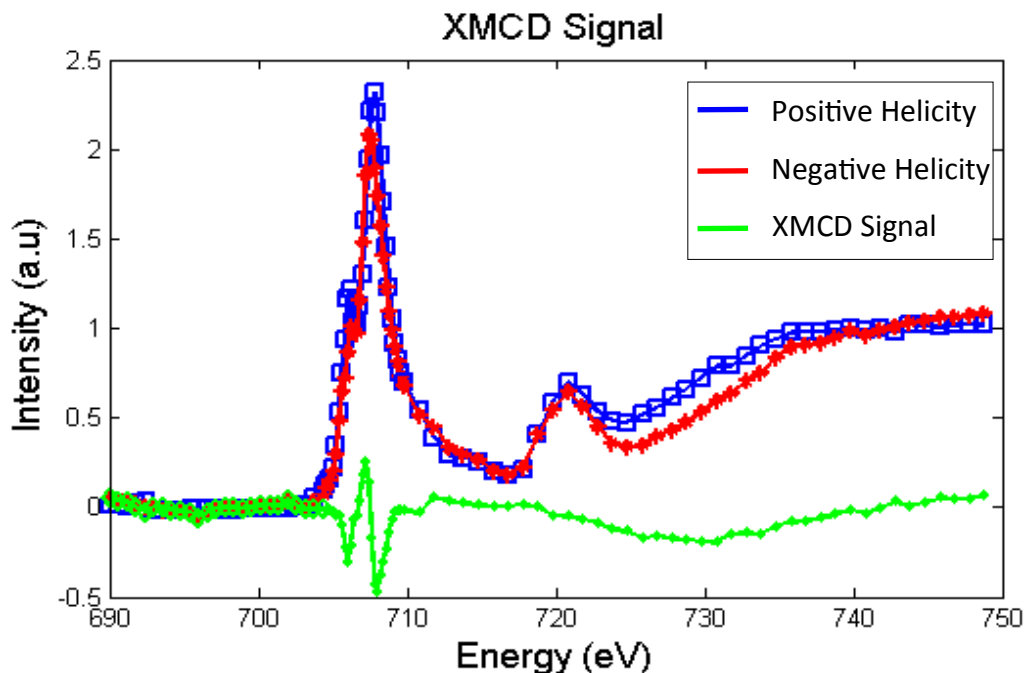


Figure 2.4 X-ray absorption spectrum of NP 17 at 300 K with positive and negative helicity of x-ray. The difference of the absorption is the residual line showing the XMCD spectrum. The W shape is evidence of the three magnetic moments. The three peaks in the “W” shape are three resonant energies.

The shape of the XMCD signal shown in Figure 2.4 indicates a non-zero signal, arising from the ferrimagnetic spins being excited from a core state into a valence state by the different helicity of x-rays. We notice a “W” shape at the first peak around the L_3 edge in the spectrum at 708 eV. The three peaks forming this “W” shape is a signature of the different spins for the Fe^{2+} and Fe^{3+} ions. From XMCD we noted the three energies of the three ferrimagnetic spins of magnetite, which are the three peaks in the “W” shape, are $E = 706, 707, 708$ eV. We call these energies E_1, E_2, E_3 . We later measured the XRMS signal at these specific energies.

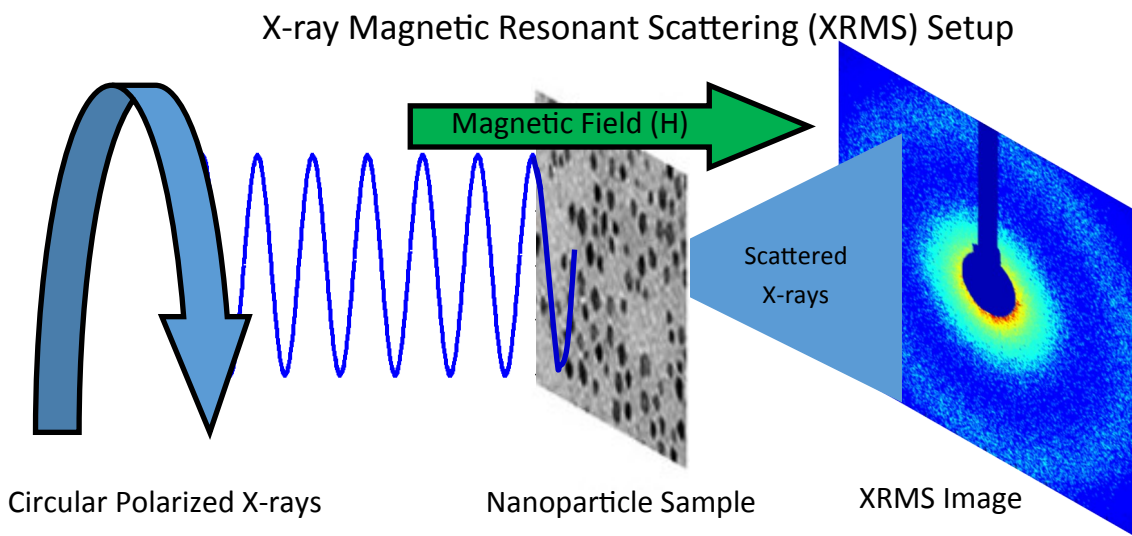


Figure 2.5 Setup for x-ray Resonant Magnetic Scattering experiment. The x-ray energy is set to either E_1 , E_2 , or E_3 to illuminate the nanoparticle membrane. A magnetic field is also applied to the sample to influence the magnetic ordering in the nanoparticles. The x-rays are scattered and captured on a CCD camera.

2.4 X-ray Resonant Magnetic Scattering (XRMS)

X-ray Resonant Magnetic Scattering (XRMS) is complementary to XMCD in the sense that we can extract spatial electronic and magnetic information from the sample. In order to use XRMS, we needed to first measure the three resonant energies E_1 , E_2 , E_3 that we found in the XMCD signal. As discussed, the magnetic signal is enhanced at these frequencies. Magnetic scattering occurs when photon spins interact with electrons. The x-ray scattered light arises from the spatial variation in the electronic structure of the nanoparticle assembly, with the rest remaining from the magnetic spatial variation. Thus, XRMS provides information about spatial structure such as the inter-particle distance and more importantly, the magnetic ordering within the nanoparticle assembly.

To collect the XRMS signal, we replaced the photodiode with a 2048 x 2048 pixel CCD camera and captured the scattered light. Instead of sweeping the energy and producing plots as a function

of energy, the x-rays energy was fixed, at either of the three different resonant energies that were found in XMCD. In Figure 2.5, a simple diagram outlays how scattering images were produced by the soft circular polarized x-rays passing through the nanoparticle assemblies. An external magnetic field was applied during this experiment. The field values recorded from $H = -3000$ to 3000 Oe. At $H = 3000$ Oe the magnetization in the nanoparticles reaches its saturation. Liquid helium was used to cool the nanoparticle sample down to various temperatures such as 20 K, 80 K, 150 K. With different field values and temperatures, the scattering pattern captured on the camera changed. We studied these changes to understand the magnetic ordering.

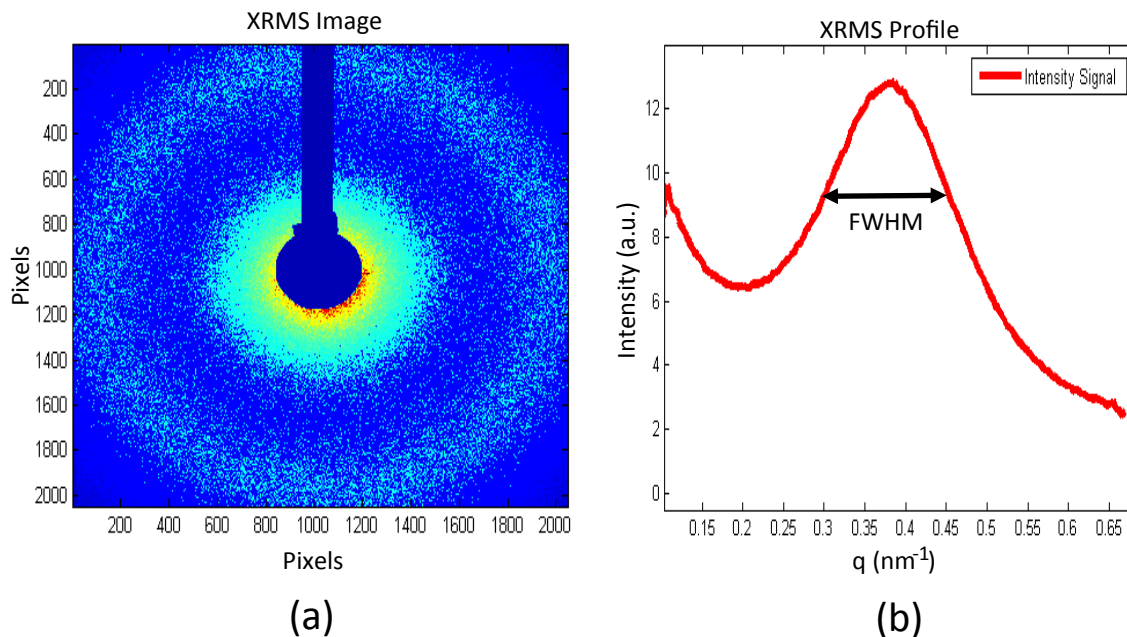


Figure 2.6 Image (a) is an image of x-ray resonant magnetic scattering. The ring is significant as it indicates the nanoparticle structure and the magnetic signal based on the position and width. The image (b) is the XRMS image converted into one dimensional profile. The line in between the peak is the full width half maximum which is the thickness of the ring.

An example of XRMS image is shown in Figure 2.6. The color indicates the amount of scattering intensity. In order to extract more quantitative information, we transformed the image into

a one dimensional profile. We do so by the following: We first subtracted the background image from the scattering image to eliminate any unwanted data. Next, in Figure 2.6 we notice a large blocker in the center. This is to block the direct x-rays damaging the camera. We first want to mask this part of the image because the intensity encompassed by the blocker is not meaningful. We remove this region by simulating a zero-blocker to multiply with the scattering image. That way, the data within the blocker region will not be included in the profile. Time and spatial normalizations were then applied. The camera was able to capture the scattering x-ray for a duration of time thus averaging the intensity over time. We then generated a ring set. As we can see in Figure 2.6, rings form on the XMRS images indicating the an isotropic signal. We located the center of these rings and used it as the origin. We then performed an angular integration of the scattering intensity using a set of concentric rings of increasing radius. The integration process produces an intensity profile $I(q)$ and the resulting profile is shown in Figure 2.6. From these one-dimensional intensity plots we extracted information about the sample structure and the magnetic ordering. The program and process is explained in more detail in Appendix A. The variable q from the Intensity function $I(q)$ represents the scattering vector, or the distance to the center and is in units of inverse nanometers. In order to calculate q , the distance between the sample and the detector needed to be first evaluated.

2.5 Finding the Distance to Detector

Hundreds of profiles were created. Each profile was created at different energies, temperatures, helicity of light, and at different magnetic field strengths. These profiles are what we will later model to extract information about the magnetic ordering. In order to compare the experimental data with a model we need to convert the pixel position of the scattering signal on the CCD into scattering vector q expressed in nm^{-1} , the conversion from pixel to SI units is one pixel = $13.5\mu\text{m}$.

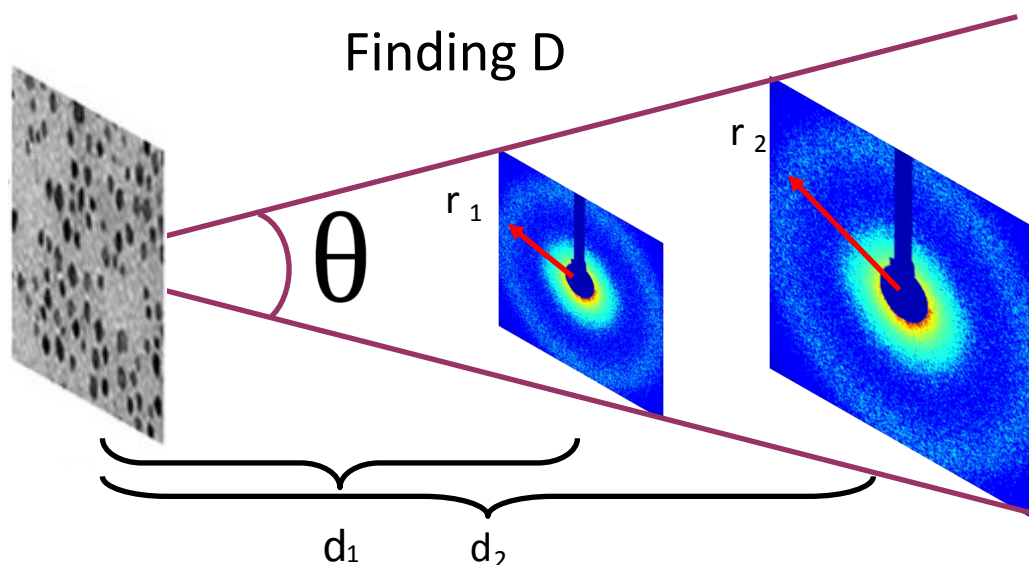


Figure 2.7 Diagram demonstrating how the distance D was found in the vacuum chamber. We used a simple ratio relationship to acquire the distance from the nanoparticle distance to the camera. This distance was critical to know the radius on the ring in the XRMS images.

Other features including the distance from the sample to the camera needed to be calculated. We call this distance D . These parameters are useful to calculate the scattering vector q in nm^{-1} as q is inversely proportional to D shown in equation 2.4. Measuring D required a complex process because the vacuum chamber prevented us from measuring the distance directly using calipers.

We determined D by comparing scattering profiles collected at different distances. As shown in Figure 2.7, we captured two images, one at distance d_1 and another at distance d_2 . From the sample we note the difference between the two positions as Δd . It turns out that Δr is proportional to Δd according to equations 2.1-3. At d_1 , we measured the peak at r_1 and at distance d_2 , we measured the peak at r_2 . The equation 2.1, shows the ratio used to deduce D . The values of R and D were at the position of r_2 and d_2 . We did this estimation multiple times with three images at different locations. The estimated value for D is 105.5 mm.

$$\Delta d = d_1 - d_2 \quad (2.1)$$

$$\Delta r = r_1 - r_2 \quad (2.2)$$

$$D = R \left(\frac{\Delta d}{\Delta r} \right) \quad (2.3)$$

For the rest of the XRMS measurements, the camera was placed at distance D from the sample. Knowing the distance D , we now can calculate the q value that corresponds to the pixel positioning on the CCD camera. To begin, we first needed to know the energy E of the x-rays that scattered from the sample. The energy E was recorded at $E = 708$ eV, with an associated wavelength λ of the x-rays $\lambda = 1.76$ nm. Next, we measured the pixel number of the peak position R by finding the maximum value and converted into SI units. By knowing R and D values we determined $\sin(\theta)$ using equation 2.4, from which we could evaluate q . The q value is the positions peak in the inverse space and has the units of nm^{-1} .

$$q = \frac{2\pi}{\lambda} * \sin(\theta) \quad \text{where } \lambda = \frac{hc}{E} \text{ and } \sin(\theta) = \frac{R}{D} \quad (2.4)$$

We then use Bragg's diffraction law in equation 2.5 to transform the q value into the real space. This transformation declares the average size of the nanoparticles along with the interparticles spacing P of the nanoparticle assembly and is recorded in table 2.1.

$$P = \frac{\lambda}{\sin(\theta)} = \frac{2\pi}{q} \quad (2.5)$$

2.6 XRMS Profiles

After plotting the intensity $I(q)$ of the scattering profiles and performing some calculations, we were able to make some conclusions about each of the nanoparticle samples. By finding the dis-

tance D to detector we were able to obtain the peaks position in each sample's profiles. The peaks position is produced by the charge intensity scattering by the x-rays and indicates the average nanoparticle size and interparticle distance of the nanoparticle assembly. The width of the peak is also of interest, the full width half maximum (FWHM) of each sample was determined, the distance is represented in Figure 2.6. The FWHM indicates the distribution of the nanoparticles assembled on the membrane. The bigger the value for the FWHM, the larger the distribution of nanoparticles. The values for the FWHM were then used to find the correlation length CL for each sample. As the FWHM is measured in the inverse q space, the value is inverted to know the correlation length. If the distribution is large, the correlation length will be short. The equation for correlation length is $CL = 2\pi/FWHM$. The table 2.1 below shows our results from our findings.

XRMS Approximate NP Sizes Table							
Sample	NP	Size(nm)	q_p (nm^{-1})	P (nm)	FWHM (nm^{-1})	CL (nm)	CL/P
Sample 1	NP16	11	0.32	19.77	0.102	61.3	3.1
Sample 2	NP16	11	0.30	20.54	0.113	55.3	2.7
Sample 3	NP16	11	0.38	16.57	0.128	49.0	2.9
Sample 4	NP17	8	-	-	-	-	-
Sample 5	NP17	8	-	-	-	-	-
Sample 6	NP17	8	-	-	-	-	-
Sample 7	NP18	5	1.02	6.11	0.253	24.83	4.0
Sample 8	NP18	5	1.00	6.31	0.256	24.51	3.9
Sample 9	NP18	5	1.01	6.18	0.278	22.58	3.7

Table 2.1 A quick analysis was done of each of the samples to find the particles diameter and the interparticle distance. These numbers are just estimates to assist us with the modeling that occurs in chapter two. Sample 4 through 6 are not included because of the weak signal in their XRMS profiles.

When the nanoparticles are sparsely distributed on the membrane, the interparticle distance is significantly larger than the diameter of the average nanoparticle. For samples 1 through 3 the interparticle distances are about twice as big as the particle diameter, whereas for samples 7-9, the interparticle distances are only slightly bigger than the particle diameter. The numbers found in Table 2.1 are preliminary estimates and will be useful for modeling purposes. We should find a strong correlation between these results and the models.

2.7 Dichroic Signal

A magnetic signal was extracted from the XRMS measurements by exploiting the polarization. In Figure 2.8, we present the XRMS profiles of NP16 at 80 K and at a field value of $H = 1000$ Oe. We observe that the intensity is much higher for the positive helicity compared to the negative. The difference in the intensity is proof of the magnetization component of these nanoparticles. Though the charge scattering signal dominates the magnetic signal in these scattering profiles, the difference in the intensities of the scattered x-rays is proportional to the net magnetization of the nanoparticle assembly. To only study the magnetic signal from these XRMS profiles, we subtract the intensities from one another. This is called the dichroic effect. We use two ratios to obtain our magnetic signal, called the dichroic ratio R_d and the magnetic ratio R_m , defined in equations 2.6 and 2.10. Figure 4.5 shows the magnetic ratio at different external magnetic field values. I_+ and I_- are the intensities from the positive and negative helicity.

$$R_d = \frac{I^+ - I^-}{I^+ + I^-} \quad (2.6)$$

$$R_m = \frac{I^+ - I^-}{\sqrt{I^+ + I^-}} \quad (2.7)$$

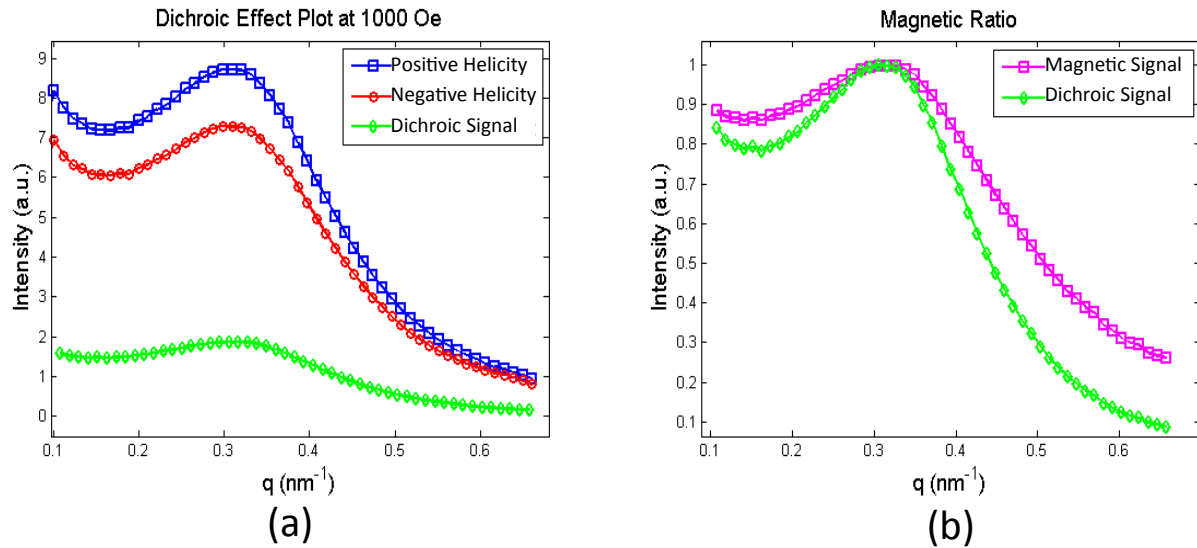


Figure 2.8 The plot (a) shows the intensity from the positive and negative helicity of x-rays on the nanoparticle sample. The positive intensity is greater than the negative because of the stronger interaction of the x-rays and the nanoparticles. The difference of these helicities is given as the green line and is called the dichroic effect. Plot (b) is the magnetic and dichroic ratios plotted.

Based on the helicity of the x-rays and the external magnetic field, the magnetic ratio accounts for the interaction of these two changes. We notice that at higher field value, the magnetic ratio of x-rays has a stronger magnitude. The intensity of the magnetic ratio is proportional to the magnetization of the nanoparticles. As the field value decreases and even goes negative, the magnetic ratio also changes sign. This flipping occurring indicates a flipping in magnetization opposite as the external magnetic field begins to change its sign. The position of the peak occurring in Figure 2.9 indicates the magnetic period in the nanoparticle assembly. We notice that individual peaks are moving closer to the $q = 0$ as the external magnetic field gets weaker in magnitude. Therefore, the magnetic period in the sample is changing due to the external magnetic field.

If all of the nanoparticles' spin configurations are aligned in the same direction, then we call this ferromagnetic ordering and is presumed to be present when the external magnetic field is strong. This ferromagnetic ordering is visible in the blue and green curve in Figure 2.9 for sample

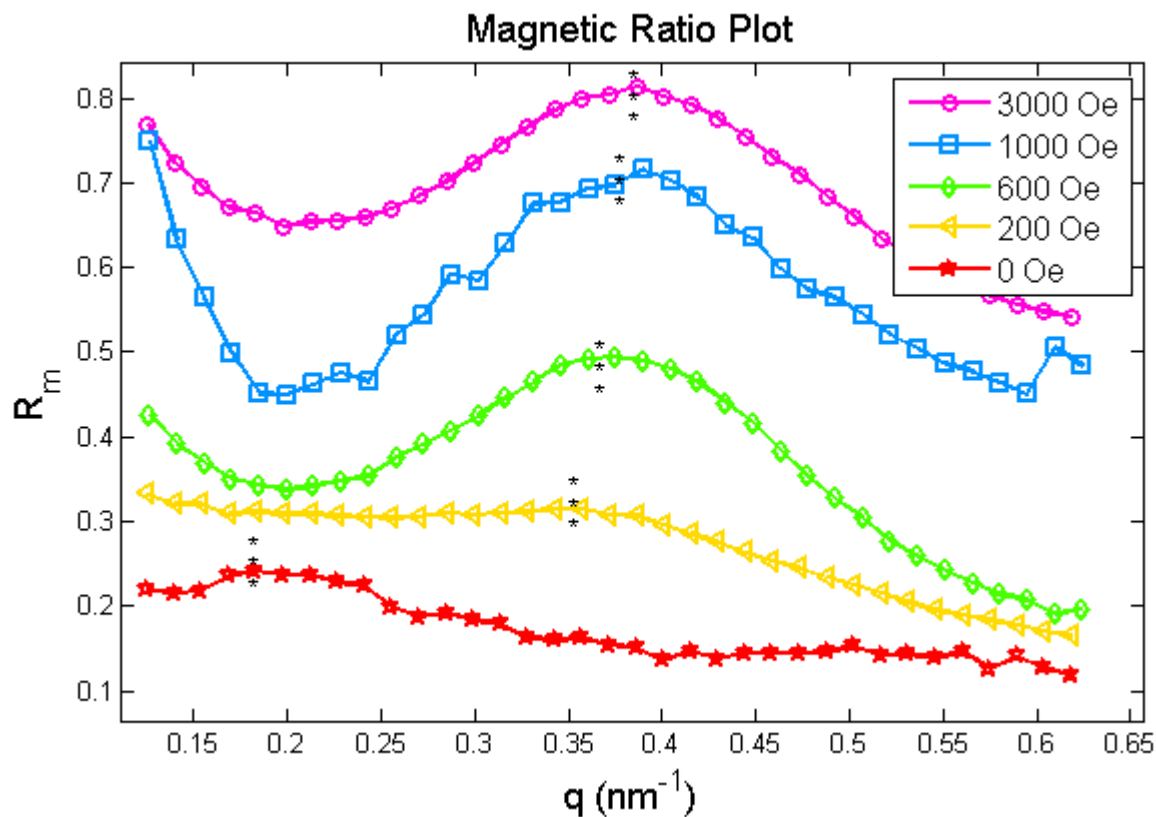


Figure 2.9 The dichroic effect technique was used on sample 3 at room temperature $T = 300 \text{ K}$ as it experienced different magnetic field values (H) through a magnetization loop. The magnetic ratio was then calculated, normalized, and then plotted as seen. The line asterisk indicates where the maximum point is on the plot. We can see as the field value decreases the maximum is moving toward the center.

3. Notice that these peaks are exactly at the location of the charge scattering peak seen in the XRMS profiles. When the external magnetic field is smaller, the magnetic ordering has less of a ferromagnetic component and more of the other orders such as antiferromagnetic order which is comprised of a spin-up spin-down orientation. The magnetic ordering of these dichroic effect plots will be discussed more in chapter 4 as it plays an important role in deciphering the magnetic signal.

2.8 Conclusion

In conclusion, chapter 2 outlined the experimental work for gathering information of the magnetic ordering of these nanoparticle samples. For the XAS and XMCD we scanned a range of x-ray energy to find the $L_{2,3}$ resonant edges of Fe. We presented the data for positive and negative helicity in Figure 2.4 and displayed the XMCD signal from it. The three resonance energies were detected in Fe_3O_4 due to the three ferrimagnetic spins of the iron ions.

In the XRMS experiment, we tuned the x-ray energy to the resonant edges of Fe_3O_4 and produced scattering intensity images. We found the distance D from the camera to the samples and used spatial and time normalization to convert these images into a one dimensional plot. From there we extracted information of the interparticle distance and the correlation length of the nanoparticles. Towards the end, we discussed the importance of the dichroic effect technique and how it characterizes the magnetic ordering based on the external magnetic field. We introduced the importance of ferromagnetic and antiferromagnetic ordering to describe the position of the dichroic peak. In summary, these nanoparticle samples display a strong magnetic signal and by modeling these XRMS and dichroic effect profiles we can find more information of the magnetic orientation in the nanoparticle assembly.

Chapter 3

Structural Modeling of the Nanoparticle Chain

3.1 Introduction

We constructed models of chains of nanoparticles to fit the XRMS profiles and the dichroic effect results. The purpose of modeling is to explain what is occurring in the real space. The XRMS data is measured in the inverse q space (or Fourier space). By creating a function with several parameters, we hope to fit the scattering profiles in order to understand the ordering in the real space. From the model, we determine structured parameters of each sample including the interparticle distances and correlation length. We used MATLAB to generate these models of magnetic nanoparticles. We began creating a charge density function and then later on added the magnetic components for each of the nanoparticles spin as described in chapter 4. The actual samples were deposited onto two-dimensional membranes with millions of nanoparticles in the illuminated region. For simplicity, we use a one dimensional model, being a chain of nanoparticles.

3.2 Charge Density Function

The charge density function required several parameters to represent the actual chain. We started with a few parameters such as: 1) the radius R , 2) the interparticle spacing L , 3) the number of nanoparticles N , and 4) The total number of pixels per chain. The number of nanoparticles N was set to a value around 100, as we needed enough nanoparticles to provide statistical sampling to represent our entire nanoparticle sample. The resulting period in the particle chain was set as $P = 2R + L$. In Figure 3.1, a diagram illustrates our the nanoparticle chain model.

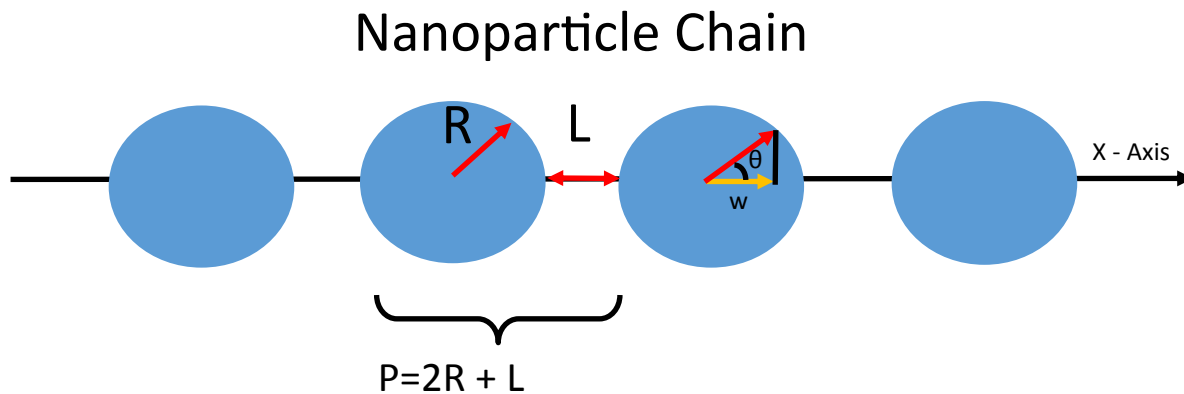


Figure 3.1 Chain of nanoparticles used for our model. The resulting charge density function included a few parameters such as the radius R and interparticle distance L , having a period of $P = 2R + L$. The density function was expressed as a function of w on the x -axis.

Figure 3.2 shows the MATLAB code we used to generate a nanoparticle chain along with a output function. The charge density function $Y(w)$ is expressed as a function of the position w on the x -axis, where $w = R\cos(\theta)$. The $Y(w)$ function is a basic projection of a slice through the nanoparticle onto the x -axis. This is done by integrating the volume of a disk of a radius $R\sin(\theta)$ and the thickness dw of the disk. Equations 3.1 shows the sequence to show how the charge density function was obtained to represent the actual nanoparticles in assembly.

$$Y(w)dw = \pi[R\sin(\theta)]^2dw \quad (3.1)$$

$$Y(w) = \pi R^2[1 - \cos^2(\theta)] \quad (3.2)$$

$$Y(w) = \pi(R^2 - w^2) \quad (3.3)$$

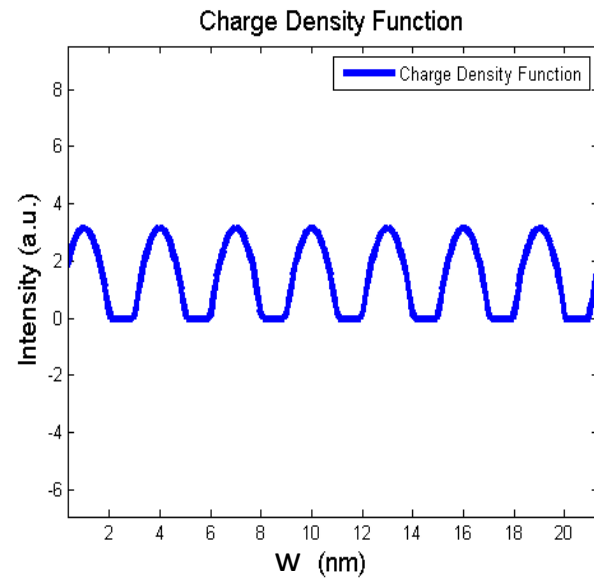
```

R = 1;
L = 1;
N = 10;
tau = (2*R+L);
x=linspace(0,N*tau,N*25);

for i = 1:length(x)
w=(x(i)-(2*R+L)*floor(x(i)/(2*R+L))-R);
    if abs(w) <= R
        y(i) = pi*(R^2-w^2);
    else
        y(i) = 0;
    end
end
figure;plot(x,y); axis equal

```

(a)



(b)

Figure 3.2 (a) Actual code to formulate the charge density function. We can see the parameters such as the radius R , interparticle distance L , the number of particles N are embedded into the function. (b) Plot of the output of the charge density function $Y(w)$.

3.3 Nanoparticle Size Distribution

After creating a basic charge density function with a unique given period P , we incorporated a distribution of various periods $P \pm \Delta P$. On the physical membrane, not all the nanoparticles have the same size and distance from each other. In Figure 3.3, we see again the TEM images for the

three NP16, NP17, and NP18 showing the variance in the sizes and interparticle distances. The histogram below each image show the distribution of particle sizes. These histograms indicate that the size distribution is narrower for smaller particles. In order to replicate this distribution in the code, we added a distribution σ_R for the radius R and σ_L for the interparticle distance L . R_c and L_c were introduced to represent the average radius and interparticle distance. These parameters symbolize how much variance would occur to the radius or interparticle distance.

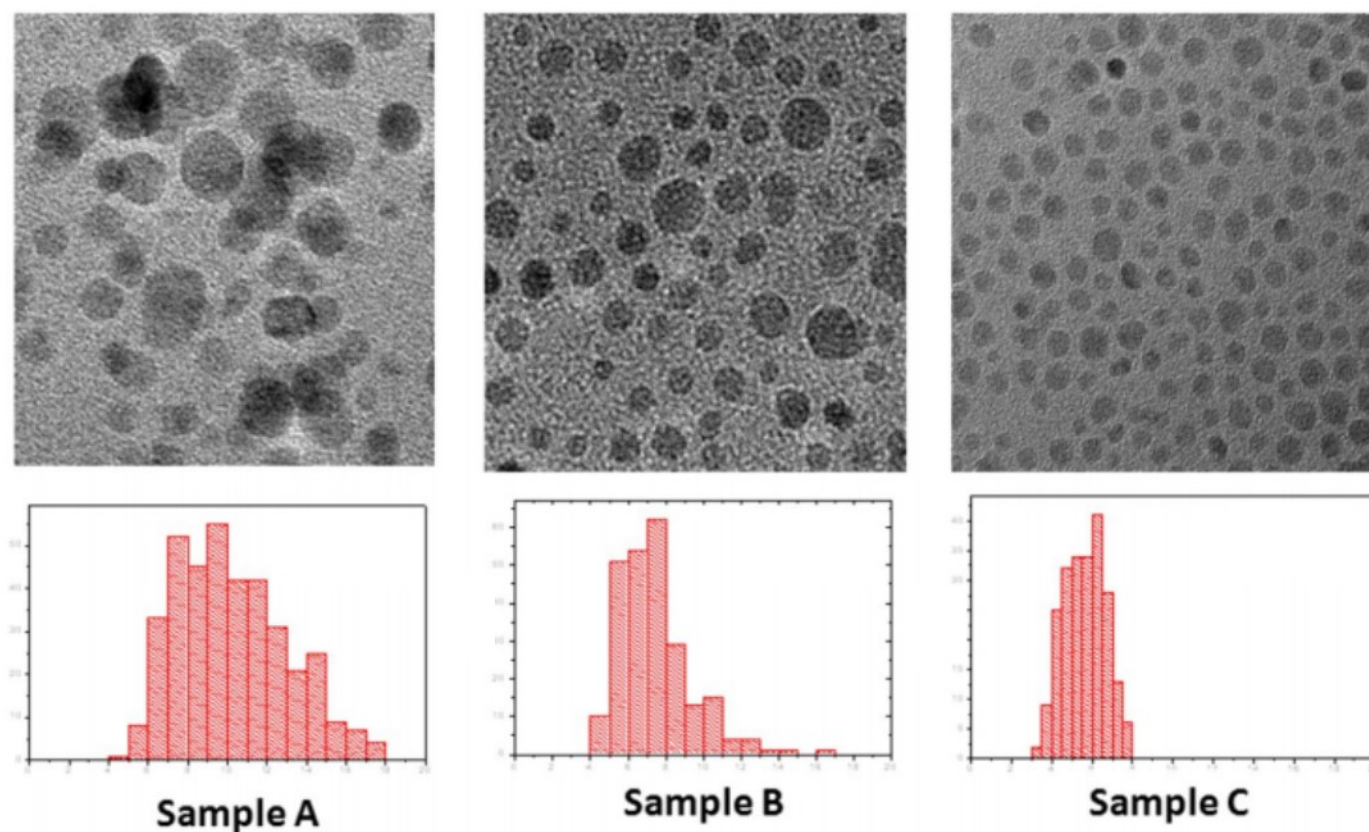


Figure 3.3 TEM images of sample NP16, NP17, NP18. Below these images are histograms to of the size distribution. We can see that as the nanoparticles are bigger the distribution widens as well. (Cai et al. 2014)

A new parameter called *Sets* was then introduced. *Sets* is a collection of function $Y(w)$ with the different ranges of L and R . The variable R varied from $R - \sigma_R/2$ to $R + \sigma_R/2$ and similarly for the L , varying from $L - \sigma_L/2$ to $L + \sigma_L/2$. Each function created in *Sets* was first summed together in equal weight and generated an average value for the radius and interparticle distances. Later on, it will be summed together following with a Gaussian distribution to reproduce the actual size distribution in our samples.

3.4 Scattering Intensity

After creating a function in the real space, we needed to transform the function into the inverse space to simulate the scattering signal. We ultimately needed to produce a plot of the scattering intensity, $I(q)$. The simulation is then used to fit the profiles produced in the XRMS data. The individual nanoparticles assembly creates a “lattice“ structure and the placement of each particle within the lattice has a period P that depends on the size and distance between each particle. The Fourier transform of the charge density function converts the function into the inverse space and create peaks based on the periods in real space. The scattering intensity that was used to convert the charge density function into the inverse space is given by the following.

$$I(q) = \left| \int_{-\infty}^{\infty} I(w) e^{i2\pi qw} dw \right|^2 \quad (3.4)$$

The peaks created in the inverse space tells us the periods occurring in the real space. For each summed function, the peak position in the inverse space should occur around the average period which should be around $P_C = 2R_C + L_C$. The width of the peak was determined by how wide the values of σ_R and σ_L were combined. For the model to be on the same scale as the experimental data, the chosen range for q was crucial. In the experimental data, the intensity peaks have a seemingly Gaussian shape and the model needs to replicate that shape as well. In the summed

charged density function where we added all of the functions of different periods, we convolved to each $Y(w)$ function by a Gaussian function to replicate the scattering peaks. Normalization was applied to the model function and the first order peak of the experimental data was set to the value of one.

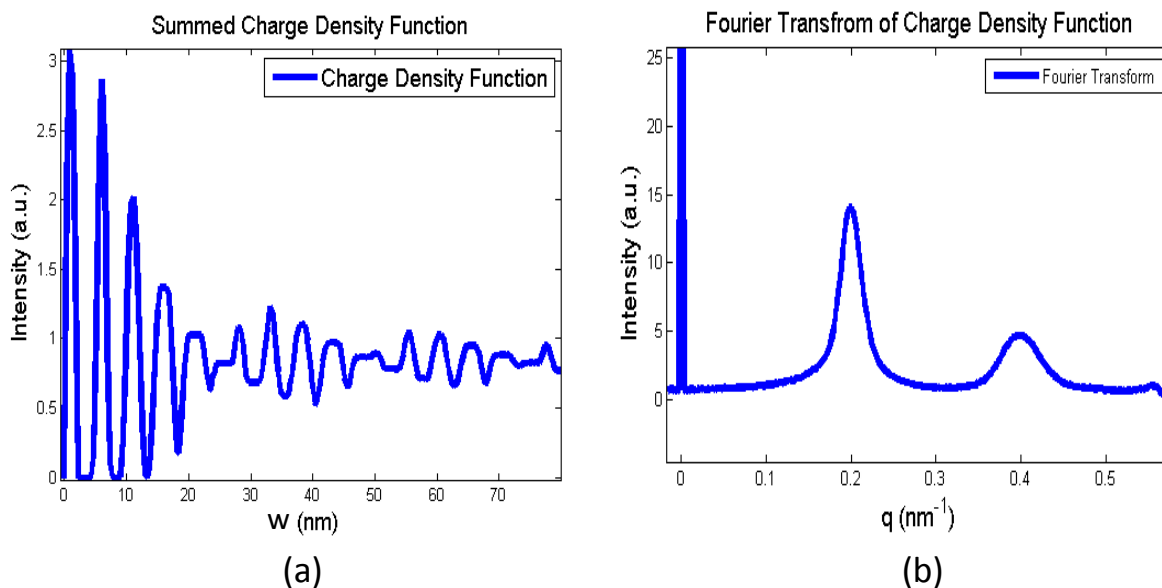


Figure 3.4 (a) Summed charge density function with the following parameters $L_C = 6.5$, $\sigma_L = 2$, $R_C = 5.35$, $\sigma_R = 2$, $N = 100$, and $Sets = 100$. (b) Fourier transform of the charge density function.

3.5 Results of Model Fits

After optimizing the charge density function we were ready to fit the XRMS profiles. We started to fit each of the nine samples. We knew from the XRMS data that since the charge scattering dominates the magnetic signal, we could fit one profile from each sample to obtain the sizes and the interparticle distances of the nanoparticles. We ended up only adjusting parameters L and σ_L . R and σ_R were already determined in the TEM results. These values were put into the function as

fixed parameters. While fitting the experimental data, an optimization code was implemented into the script. This was used to find the best results to satisfy this criterion by still having the peak position and width match up. Results are displayed in Figure 3.5 to show the experimental data with the model.

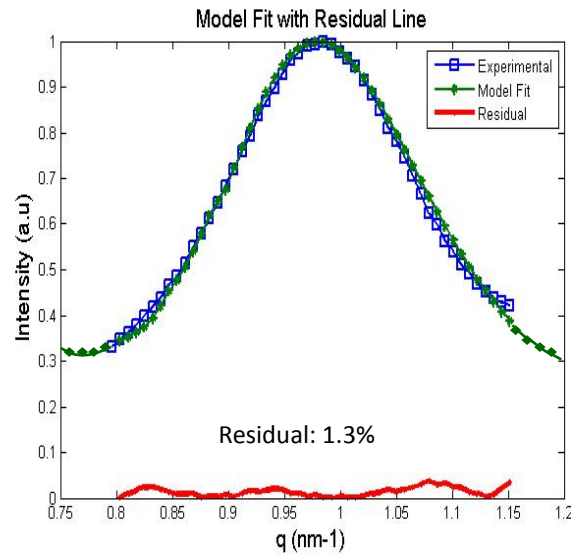


Figure 3.5 Fit of the XRMS profiles with the charge density function along with the residual signal. The residual percentage ε for this fit is about 1.3 %.

$$P_C = 2R_C + L_C \quad (3.5)$$

$$\sigma_P = 2\sigma_R + \sigma_L \quad (3.6)$$

The difference between the charge density function and experimental data was calculated for each model fit. This difference is called the residual signal and is shown in Figure 3.5. The average value of the residual signal is called the residual percentage ε . A criterion was set for a good modeling fit to have $\varepsilon < 5\%$. All the plots came fairly close and gave a residual percentage between 0.5 to 1.3 %. After fitting each of the nine samples, we assembled a table 3.1 to show

Model Fitting Table							
Sample	NP	R	σ_R	L	σ_L	$P \pm \sigma_P$	ε (%)
Sample 1	NP16	5.35	1.35	8.21	2.71	18.91 ± 5.41	1.2
Sample 2	NP16	5.35	1.35	7.76	1.46	17.63 ± 4.16	1.1
Sample 3	NP16	5.35	1.35	6.01	1.05	16.71 ± 3.75	1.3
Sample 4	NP17	3.78	0.85	3.15	0.48	10.71 ± 0.77	4.9
Sample 6	NP17	3.78	0.85	3.00	0.51	10.56 ± 1.7	4.5
Sample 7	NP18	2.75	0.5	0.63	0.21	6.13 ± 1.21	0.7
Sample 8	NP18	2.75	0.5	0.81	0.21	6.31 ± 1.21	1.3
Sample 9	NP18	2.75	0.5	0.73	0.18	6.23 ± 1.18	0.8

Table 3.1 Model fitting table for the nanoparticle assembly. The radius R and σ_R were already known values from the TEM results. The L and σ_L were values taken from model to fit the data. The fitted period is the average period for each sample with a variance constant. The last column ε is the residual percentage value and tells how good the fit is for each sample. All results except the last column are in nanometers.

the fitted values of L and σ_L . All of the fits for eight of the samples are presented in the appendix B, only one fit is shown in Figure 3.5. Sample five is missing from the table due to the lack of an intensity peak in the XRMS profiles. As mentioned above, the particles radius R and variance σ_R were already determined and thus were fixed values in the code. The fitted interparticle distance L and variance σ_L were obtained from the code. The fitted period gives the overall average period for each nanoparticle sample, as indicated by equation 3.5. and the total variance is given by equation 3.7.

When we will alter develop the magnetic ordering and start to draw conclusions about magnetic properties, we will want to correlated the magnetic signal to the average size of the nanoparticles

on a membrane. In essence, we will be referring to this table for future use.

3.6 Temperature Dependence Study

While making these models for the nanoparticle samples, we wanted to test if the temperature affected the structural properties. It's possible that under cooling, these nanoparticles would contract or expand. If the nanoparticle changed sizes, it would change the location of the XRMS peak because of the change in the average period of the nanoparticle lattice. If the temperature did affect the nanoparticle assembly structure, we would need to account for that displacement. Ultimately the fitting the XRMS is to characterize the magnetic macro-spins of the nanoparticles. If the nanoparticle structure is changing, the change in the XRMS peak positions need to be accredited to both the charge density function and the magnetic spin function. In Figure 3.6, we plotted two samples at two extreme temperatures, both at (zero field value) $H=0$. If the experimental data was shifted, it would indicate that the structure of the nanoparticles was contracted or expanded under the presence of temperature. In Figure 3.6, we plot two XRMS profiles at 15 K and at room temperature 300 K for samples 3 and for sample 9. We concluded that the temperature does not significantly change lattice structure of the nanoparticle assembly in none of these two samples.

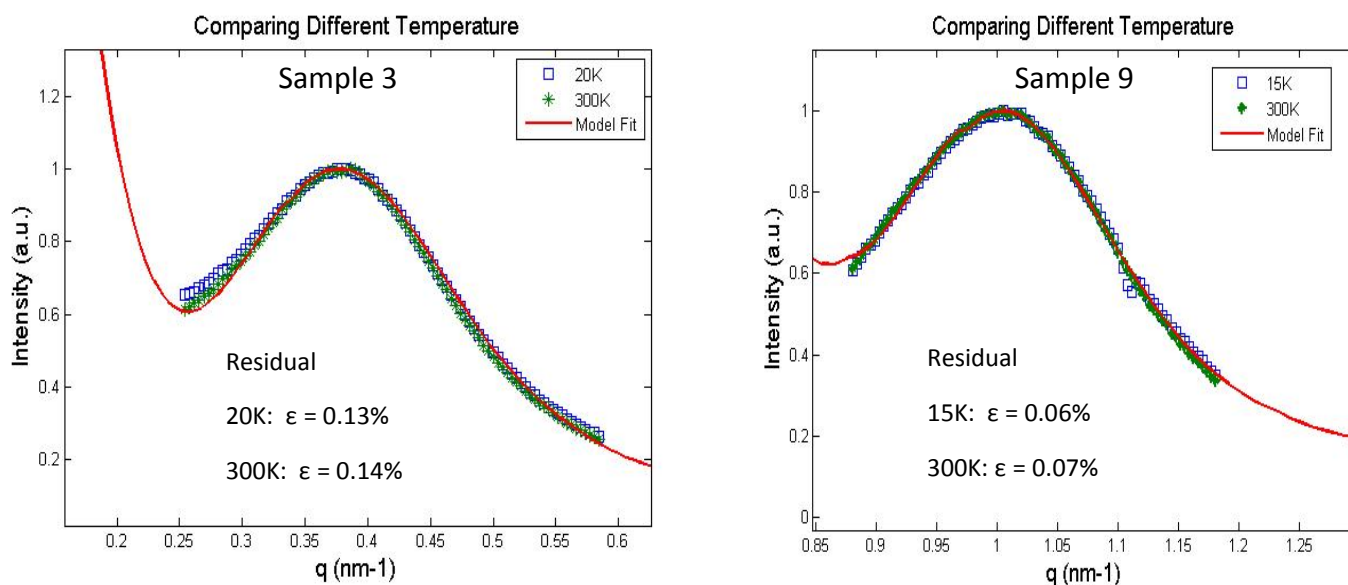


Figure 3.6 Comparison of scattering profiles collected at 300 K and 20 K for sample 3 and at 300 K and 15 K for sample 9. The difference is almost imperceptible as it only changed by a tenth of a nanometer. Changing the temperature did not have an impact on the structure of the nanoparticles and thus not affecting the scattered pattern in the profiles. The residual percentages for given for each profile at different temperatures.

Temperature Effect on Sample 3 and 9			
Sample	Temp (K)	P_c (nm)	ϵ (%)
Sample 3	20	16.81	1.3 %
Sample 3	300	16.76	1.4 %
Sample 9	15	6.17	0.6 %
Sample 9	300	6.18	0.6 %

Table 3.2 The table shows the comparison of sample 3 and 9 at two different temperatures. The model fit was able to obtain the average period P and then the residual percentage value is given as well.

Chapter 4

Modeling of the Magnetic Ordering

4.1 Magnetic Spin Function

Using the charge density function to model the XRMS profiles allowed us to make conclusions about the sizes and distributions. Next, we incorporate the magnetic spin function into the charge density function. There are two origins for the scattering signal: first, the charge scattering due to the structure of the sample and second, the magnetic scattering due to the magnetic ordering. We now look at the magnetic signal, which is basically given by exploiting the dichroic effect as described in Chapter 2. Figure 4.1 show a series of dichroic signal recorded at different field values for sample 3. We notice that the intensity of the magnetic signal decreases when the external field decreases. More importantly, the peak position is shifting towards the center as this process occurs. We want to model this shift in the peak.

To account for the magnetic ordering in the nanoparticles, a sketch is included to illustrate the behavior of what we want to model. In Figure 4.2, four types of magnetic ordering are represented, as well as their respective Fourier transforms. The Fourier transforms show a peak shifting based on different periods in the magnetic ordering. The first magnetic ordering is called the parallel

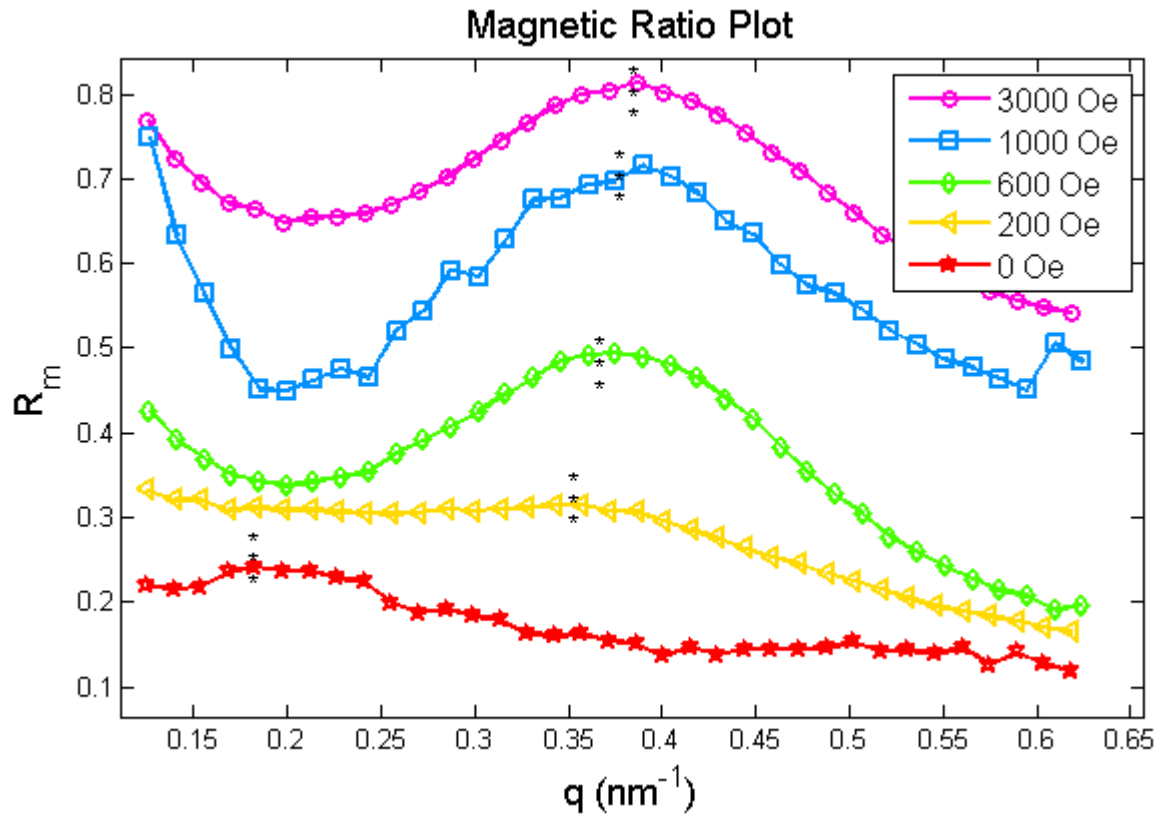


Figure 4.1 Series of dichroic signals recorded of sample 3 at $T = 300 \text{ K}$ as it experiences at different external magnetic field values of decreasing magnitude.

ordering v_1 . The Fourier transform of the parallel order is the blue line. We observe that the period in the parallel ordering creates a peak at the location q^* of the charge scattering peak. The sketch below the parallel order is called the anti-parallel ordering v_2 . In this order, the spin direction is flipped every other nanoparticle. Since the period is twice as long as the ferromagnetic ordering the peak in the Fourier transform appears halfway in between the origin and the ferromagnetic peak at $q^*/2$. Two other orderings are included called the triple ordering v_3 , which has the spin configuration of $(\uparrow, \uparrow, \downarrow)$, and the quadrupole ordering v_4 , which has the spin configuration of $(\uparrow, \uparrow, \uparrow, \downarrow)$. The first order peak in the Fourier transform are at $q^*/3$ and $q^*/4$ respectively of these orders come closer to $q = 0$ due to the larger period in their order.

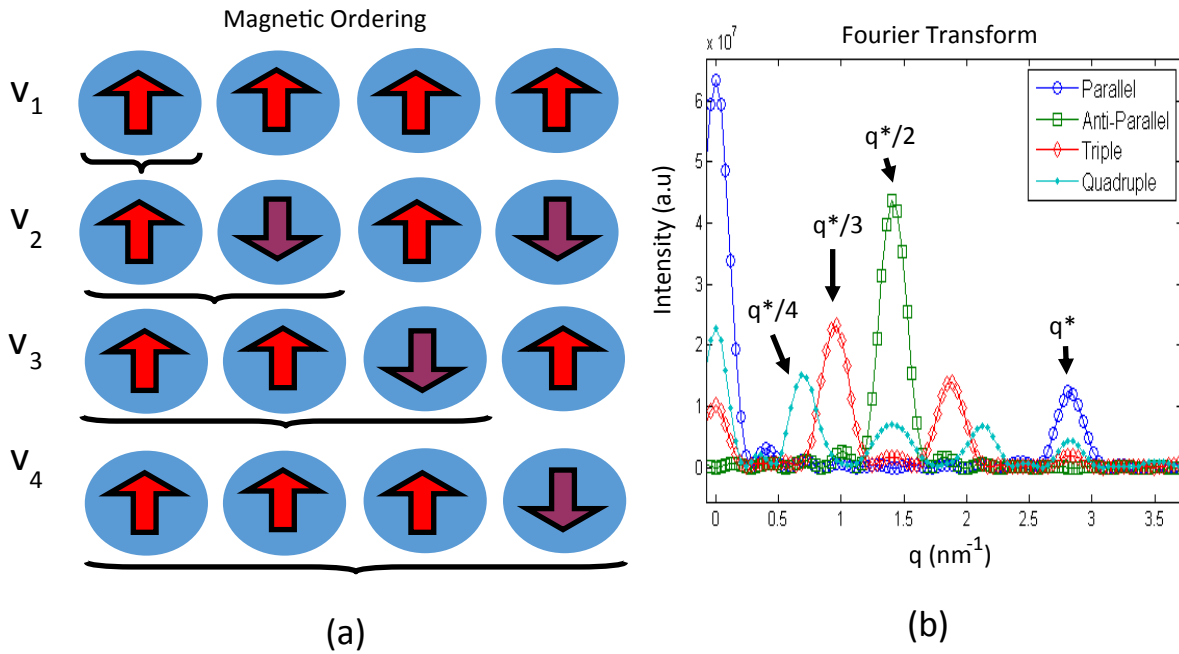


Figure 4.2 (a) Diagram showing the different magnetic orderings: parallel v_1 , anti-parallel v_2 , triple v_3 , and quadruple v_4 . Below each magnetic ordering shows the length of the period. (b) Fourier transform of the different magnetic ordering. We can see the peak shifts toward the center as the period is extended.

This observed peaks shifting is based on the spin configuration and is what we need to incorporate into the magnetic spin function. In the magnetic spin function, we make combinations of these four orderings to account for different magnetizations of the nanoparticle assemblies. For the four different magnetic orderings, we created weight coefficients to make this linear combination such as c_1 , c_2 , c_3 , c_4 . A function, *Order* was created by the combination of the weights and the magnetic ordering as follows:

$$Order = c_1 * v_1 + c_2 * v_2 + c_3 * v_3 + c_4 * v_4$$

Next, we included this magnetic spin function into the charge density function and called it the “charge spin function“. we must incorporate both the magnetic spin function and the charge density function in order to reproduce the entire XRMS signal.

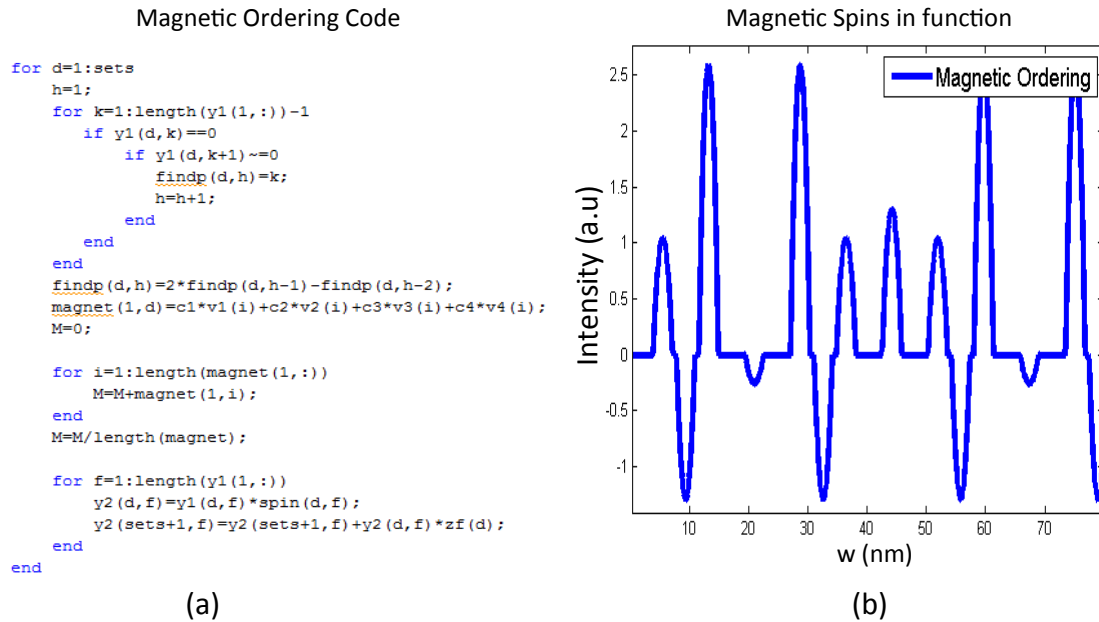


Figure 4.3 Image (a) displays the code written to incorporate the magnetic ordering to the charge density function. Image (b) is the output of the code and we can see each particle has a spin with different magnitudes in opposite directions.

4.2 Setting Constraints

Before we started to model the experimental data, two conditions needed to be considered. The first condition was the normalization and second was adding constraints to the function for optimizing the charge spin function to find the best fit. The magnitude of the XRMS signal varied with applied field, but we decided to normalize the experimental data by setting the maximum value of the magnetic order peak in the dichroic effect plots to one. In our analysis, the peak formed in the charge spin function is normalized to a value of one. We went to ease comparison of the model fit to the magnetic ratio by generating magnetization loops that were measured by a vibrating sample magnetometer (VSM) and shown in Figure 4.4 .

The magnetization loops are useful because they indicate the actual net magnetization of the sample is for a given external magnetic field. In the magnetization loop Figure 4.4, we see the

saturation occurring about $H_s = 3000$ Oe. We normalize the magnetization at saturation to $M_s = 1$. This allowed us to refer to the magnetization as a percentage.

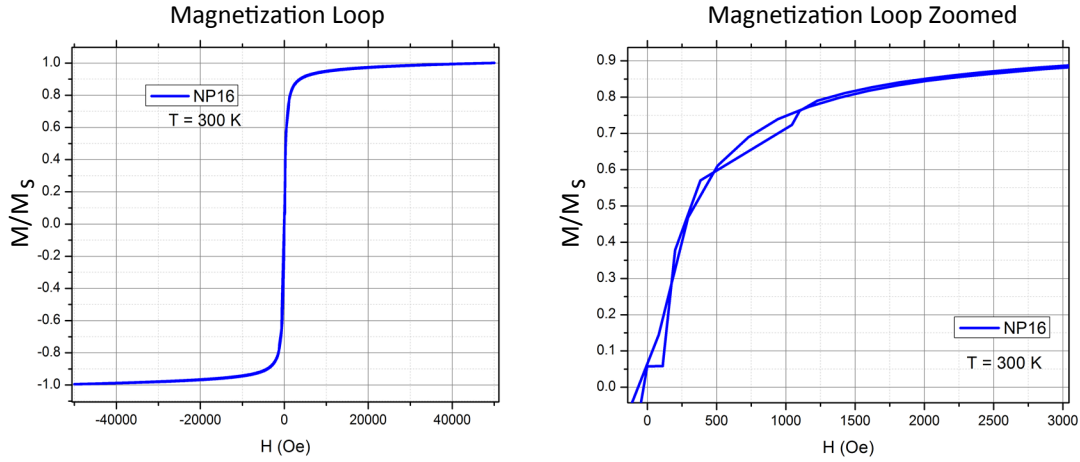


Figure 4.4 Magnetization loops measured via VSM. The y-axis was normalized and gives the percentage of the magnetization. The right images is just a zoomed image of the right as the external magnetic field only reached $H = 3000$ Oe at the synchrotron. These images were data collected from a vibrating sample magnetometer (VSM).

A couple constraints were made to ease the process of what values to use for the weights of the different magnetic ordering. The first constraint that was set, was that the magnetization is symmetrical across the origin. There was no purpose in modeling the negative magnetization compared to the positive magnetization assuming it is symmetrical. Figure 4.4 shows the magnetization loop and its symmetry allowing the magnetization occurring from $0 < M < M_s$

In the model, we wanted to calculate the net magnetization M and match it to the measured magnetization percentage M/M_s . To accomplish this $M = \Sigma Order/N$. We call this value M short for the calculated magnetization. Since the values in v_1, v_2, v_3, v_4 are either \uparrow or \downarrow and if we constrain the sum values for our weight coefficients c_1, c_2, c_3, c_4 to the value of one then the magnetic order will produce a value from zero to one. Therefore, the first constraint in the model as well is:

$$\sum_i c_i = 1 \quad (4.1)$$

Different magnetic orderings give different amounts for the overall magnetization thus altering the value of M_c . For example, if c_2 has the value of one and equation 4.1 is applied then c_1, c_3, c_4 must be zero. When we run our code to produce a magnetic ordering a value of M_c then it will sum the anti-parallel array, v_2 . This ordering of v_2 looks like $\uparrow, \downarrow, \uparrow, \downarrow$ and so on. The summed value of this array is zero and gives no contribution to the M_c value. A equation 4.2 below shows the contribution of each magnetic ordering to the overall magnetization of the nanoparticles and the overall equation for the M_c based on absolute weights of each ordering.

$$M_c = c_1 + \frac{1}{3}c_3 + \frac{1}{2}c_4 \quad (4.2)$$

4.3 Magnetic Spin Function Results

Using the above constraints, we combined with the other equations, we have four unknowns and two basic equations, leaving us with two unknowns. This greatly diminishes the amount of guessing that would occur if there were still four unknowns. We are now ready to start modeling the dichroic effect plots with the charge spin function. For the experimental data, the dichroic effect plots were already made using the magnetic ratio back in equation 3.4 and then normalized to one. Like the charge density function, the charge spin function underwent a Fourier transform and then we took the absolute value of it and squared it as shown in Figure 4.5. After incorporating these conditions the charge-spin function was applied to the experimental data, the dichroic effect plots.

The magnetic spin constants such as the parallel, anti-parallel, triple, and the quadruple ordering coefficients were determined as models were made for all of the dichroic effect plots. The model provides information about the specific magnetic configuration in the nanoparticle assem-

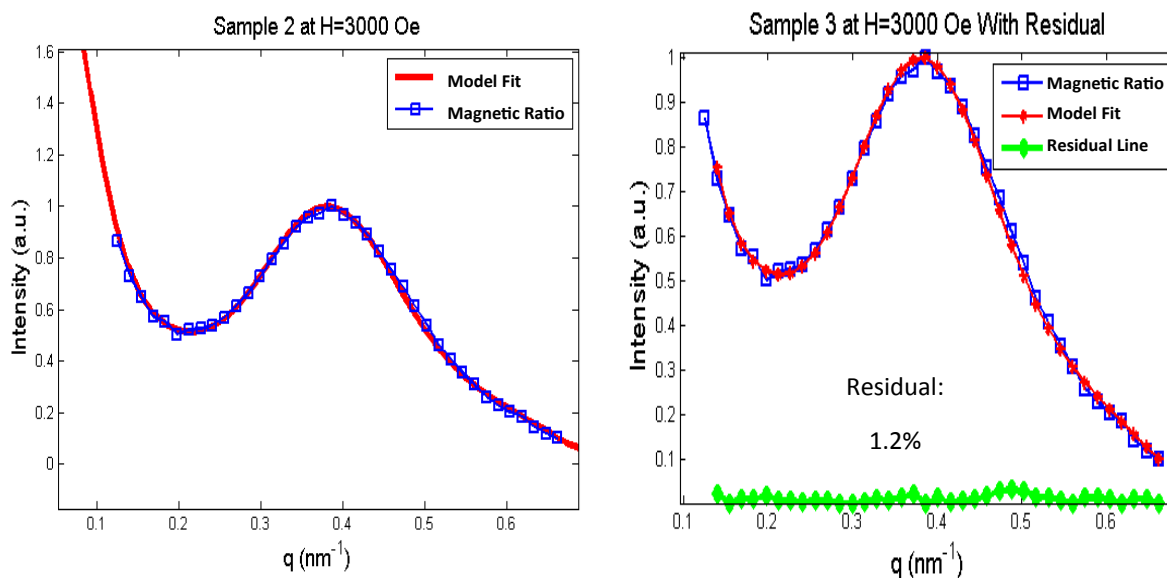


Figure 4.5 Magnetic ratio profiles fitted with charge spin function. The models were performed on a Sample 2 through a magnetization loop starting at $H = 3000$ to $H = -3000$ Oe. Other model fits are shown in appendix B.

blies for each sample. The coefficients and the distribution of the magnetic ordering chosen in the model determined this specific configuration. All models used some linear combination of these four coefficients to reenact this magnetic signal. From this combination and distribution we made conclusions about how the magnetic ordering changes as it experiences an external magnetic field. Table 4.1 lists all the magnetic ordering coefficients in the nanoparticle chains as well the M/M_s value from the magnetization loop. The M_c calculated by coefficients using equation 4.2 and the distribution of magnetic orderings. A residual percentage is also given ranging, from 0 to 3 percents. The information for the table 4.1 and 4.2 come from the model fits presented in appendix B.

Looking at Figure 4.6, it is clear that at high external magnetic fields, the parallel coefficient c_1 has the highest value, while the other coefficients descend close to zero. We conclude that the nanoparticle assembly forms a ferromagnetic order, at high field values. Looking the other

Model Fitting for Dichroic Effect: Sample 2							
Field (H)	M/M_s	C_1	C_2	C_3	C_4	M_c	ε (%)
3000	0.89	0.78	0.10	0.00	0.12	0.84	0.90
1000	0.70	0.60	0.20	0.10	0.10	0.68	0.89
600	0.62	0.50	0.20	0.15	0.15	0.62	0.95
400	0.55	0.50	0.26	0.24	0.00	0.58	0.92
200	0.33	0.18	0.28	0.26	0.28	0.41	3.34
100	0.15	0.08	0.32	0.30	0.30	0.33	1.04

Table 4.1 Coefficients and magnetization values from the charge spin function and the magnetization loop as the nanoparticle assembly experienced different field values for sample 2. M is the actual measurement from the VSM at a given field value. The coefficients are the weights for the various magnetic ordering and gave the best fit for each profile. M_c is the calculated magnetization from the model

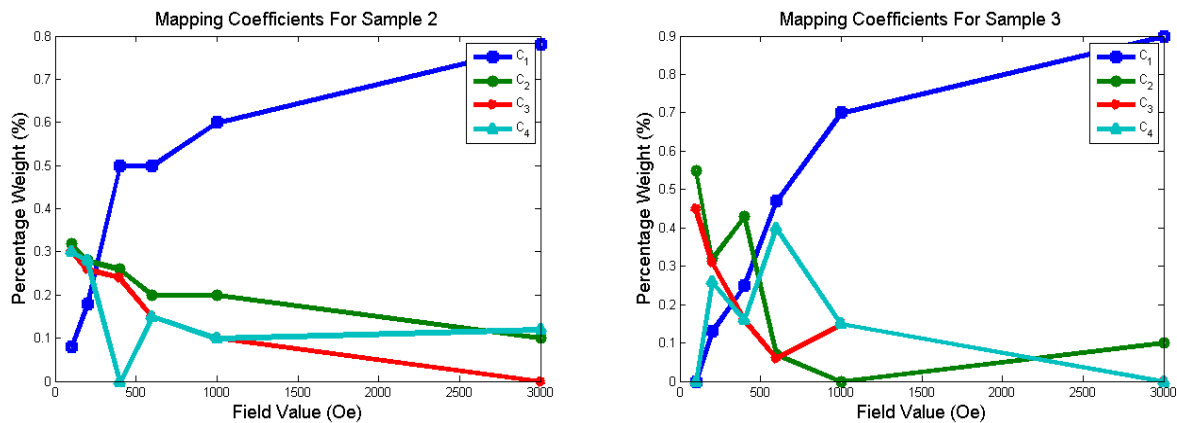


Figure 4.6 This is a plot of the coefficients from table 4.1 and 4.1. The plot presents the linear combination of the magnetic ordering as the nanoparticle assembly experiences a change in the external magnetic field.

direction, as the external magnetic field decreases the c_2 , c_3 , c_4 coefficients gradually increase at a somewhat similar rate. This is interesting to note that c_2 does not reflect what c_1 did as the field

Model Fitting for Dichroic Effect: Sample 3							
Field (H)	M/M_s	C_1	C_2	C_3	C_4	M_c	ϵ (%)
3000	0.89	0.90	0.10	0.00	0.00	0.90	0.86
1000	0.70	0.70	0.00	0.15	0.15	0.82	15.3
600	0.62	0.47	0.07	0.06	0.40	0.69	5.72
400	0.55	0.25	0.43	0.16	0.16	0.39	11.77
200	0.33	0.13	0.32	0.31	0.26	0.36	4.05
100	0.15	0.00	0.55	0.45	0.00	0.15	17.67

Table 4.2 Coefficients and magnetization values from the charge spin function and the magnetization loop as the nanoparticle assembly experienced different field values for sample 3. M is the actual measurement from the VSM at a given field value. The coefficients are the weights for the various magnetic ordering and gave the best fit for each profile. M_c is the calculated magnetization from the model

value increased. This indicates that at a zero magnetic field value, the nanoparticle assembly does not have a pure antiferromagnetic order of $\uparrow, \downarrow, \uparrow, \downarrow$ as it might have been perceived in that way. But rather a complicated linear combination of c_2, c_3 , and c_4 .

Tables 4.1 and 4.2 give the coefficients for the weights of the individual magnetic ordering for the different magnetization of the nanoparticle sample. These comparisons confirm the phenomenon of superparamagnetism as the magnetic ordering becomes ferromagnetic as an external magnetic field is applied. More work will need to be carried out to analyze the magnetic ordering of the Fe_3O_4 nanoparticles. In chapter 3, it was stated that hundreds of profiles were generated. These profiles along with their dichroic plots will need to be fitted with a model to further understand the magnetic ordering. We will understand better how external magnetic field, temperature, and nanoparticle sizes affects the magnetic ordering of each sample and thus draw more conclusions.

Future work includes improving the modeling functions to resemble the two dimensional

nanoparticle layer since the Fe_3O_4 nanoparticles is assembled on a membrane. Creating a two dimensional model would increase the accuracy and show a more physical representation.

Appendix A

XRMS Analyzing Program

This section of the thesis explains the process of analyzing the XRMS images and the program to perform such tasks. In this program, some of the functions were written by Yanping Cai, but were improved for robustness and then merged together to build a graphical user interface (GUI) to make the analyzing process more efficient and ultimately dynamic. When I first joined Dr. Chesnel's research group, I started to analyze images from the 2014 synchrotron experiment. The process was tedious and would take about ten minutes per profile. Now with this new program it can analyze the data in ten seconds or less. The program was written in MATLAB which is known for its ability to manipulate matrices quickly.

In Figure A.1, we have the basic layout to access all of the functionalities to process any XRMS images. These features include converting data files, producing blockers and ring sets, and generating 1-D profiles. Additionally, it compares the profiles for different helicities of x-rays and saves the data arrays to export to excel files. The program directly saves and uploads data files from a personal computer and organizes the XRMS profiles. This unique feature is what allows the efficiency and speed to compute these functions. Before using this program, one needs to set up a directory folder.

The program uses the "P" drive to access the data. Keep in mind that the directory in the

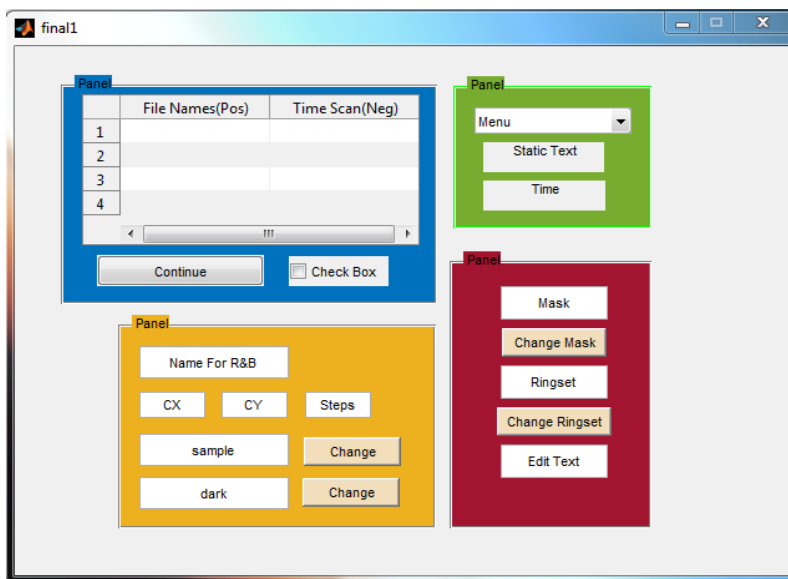


Figure A.1 The Figure displays the user interface of the XRMS analyzing program. The program is divided into four sections to convert data, create ring sets and blockers, generate profiles, and compare data.

program can be rewritten for convenience. First, a folder called “Profile“ was created in “MyDocuments“ under my “P“ drive. Like this:

/ : P/MyDocuments/Profiles/

The “Profiles“ folder maintains all of the data and information about the XRMS data. Inside of “Profile“ place Matlab code called “final.m“ and “final.fig“. These files are the scripts to run the program. Inside “Profiles“, create five more folders and name them “Analyzed“, “Blockers“, “Images“, “RingSets“, and “TimeScans“. With these five folders the program will select data files, perform the functionalities, and then place them in an organized manner. A Figure A.2 shows the folder directory.

All of the time scans and scattering images regardless of the type of format needs to be placed in the right folder. The time scans go in the “TimeScans“ folder and the XRMS images go inside “Images“. Now we are ready to run the program and evaluate the XRMS images to produce

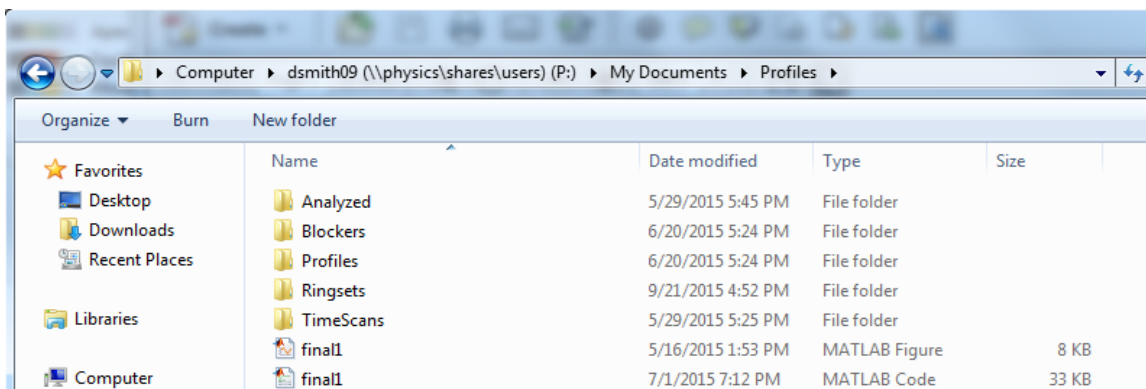


Figure A.2 The image shows the folders that need to be created in the folder called *Profiles* in order for the program to sort the data files.

profiles. To begin click on the “final.m“ file and run it, you should see a Figure A.1 pop-up. You can use the user interface to perform the needed functions. It is useful to keep the Matlab output console visible in case any error occurs. We start with the green panel in the upper right hand corner. This is called the command box. Here all of the functionalities are used to analyze the data, the other boxes are used to extract user input calls while a function is being run.

In the green panel we see a drop down menu consisting of the six functions. The six functions are “Convert SPE“, “Convert CSV“, “Make RingSet“, “Make Blocker“, “Generate“, “Compare“. Next we see an evaluation box and a time box. The drop down menu contains the functions to produce the desired profiles. The evaluation box informs the user where they are at in the computing stages. At the beginning it should say “Ready“ to inform the user that it ready to begin running a function. After a function is clicked it will change to “Running“ and then when it is completed it will say “Done“. Sometimes while a function is running the evaluation text will present “Waiting“ this means that it is waiting for a user response usually to click the “Continue“ button on the blue panel. These are the four displays for the evaluation box. The last box is the time box and it lets the user know how long it took to perform a function. The numbers are in units of seconds. Now we can begin describing what the functions do in the drop down menu, along the way we will explain the other colored panels as they are associated with the functions.

A.1 Converting SPE and DAT

The Convert SPE and CSV functions transform the data files into another file format in order for Matlab to import the data. When you click on the “Convert SPE” tab it converts the Images which have the file extension of “.SPE” and it will convert these images into “.mat” extension. The same go for the “Convert CSV” button, it transforms the files from a CSV extension into “.dat” extension. The process is easy when either function is clicked, a pop up menu will appear and display files of the images if you clicked “Convert SPE” or display the file of time scans if you clicked “Convert CSV”. You can select as many files as desired. Then click the confirm button. The pop up display will vanish and you will see the evaluation box turn from “Ready” to “Running” to indicate it’s busy processing. Also the files will be loaded in the blue panel table. The SPE and CSV files will be deleted after the conversion takes place to save memory. Each file will be named the same, just with a new file extension.

A.2 Making Ring Set and Blocker

Making a ring set and a blocker are crucial steps for generating a profile from a XRMS image. A ring set is used to do angular integration of the scattering image. A blocker can be seen in Figure A.3, it helps to get rid of any points that may occur around the center that should not be included in the integration process. Before the function is clicked a few important things need to be handled first. The first is that making ring sets and blockers use common inputs and so when you make a ring set it should always be followed by making a blocker. For example, a ring set and blocker use the same center point. Let’s look at the yellow panel and see its purpose in making a ring set and blocker.

In the yellow panel displayed above in Figure A.1 there are six text boxes that are used for making a ring set and a blocker. We divide the yellow panel into two parts to explain its purpose.

On the top half there are four text boxes labeled: “Name of R&B“, “CX“, “CY“, and “Steps.“ The “Name of R&B“ is used to give the new ring set and blocker a name. “CX“ are used “CY“ to define the center of the ring set, find these coordinates from your research lab notebook and “Steps.“ is how thick you want the rings to be. I usually use a value of eight. After these four values are defined then it is possible to proceed in making a ring set. The new ringset with its accompany name will be saved under the “RingSet“ folder. If the center of the XRMS images changes the center location then a new ring set will need to be generated. Look at the values picked to make a ring set as below

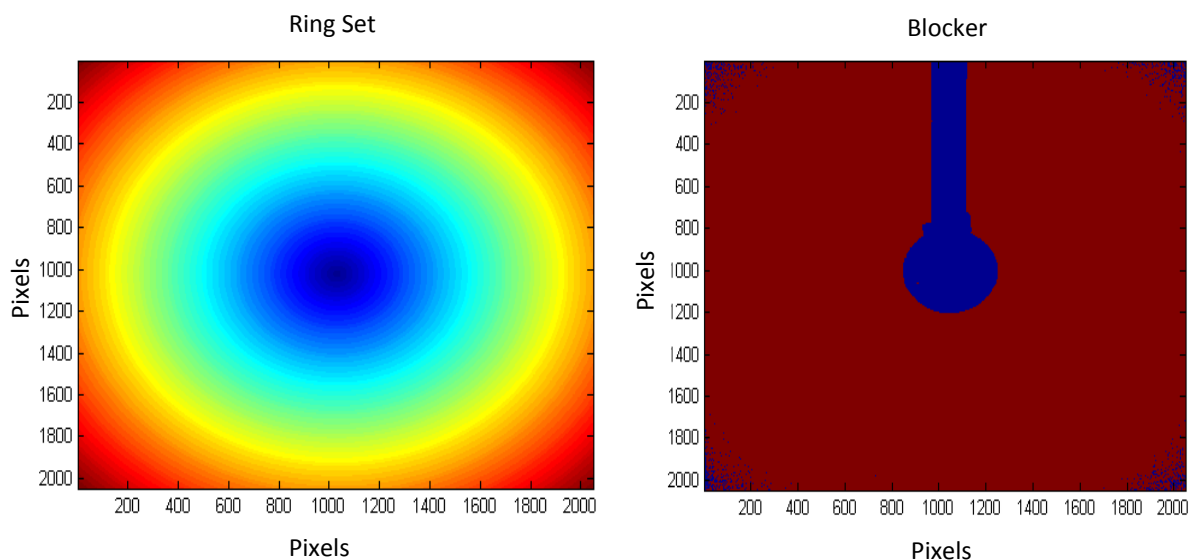


Figure A.3 On the left the image is a ring set in order to perform an angular integration. The center was chosen to be $cx = 1032$ and $cy = 1028$, with a step size of 8. On the right we have a n image of a blocker which also is part of the angular integration.

In order to make a blocker it uses the the parameters such as “Name of R&B“ and the bottom two text boxes. You will notice that in the first text box it reads “sample1_3.mat“ this is a default scattering image. To make a blocker it needs a scattering image to know where to block the center of the images and how big the blocker should be. The last box is the dark field box, this is used to subtract from the scattering images to subtract background light. Before the subtraction is

taken place, each of the dark field and scattering image matrices are individually summed. These matrices are three dimensional matrix and summing it will convert it into a two dimensional matrix.

Once this process is completed, the procedure of making a blocker is in pursuit by having a set criterion of 280. If the values in the matrix are above this criterion then they are set to the value of one. If the values are less than the criterion then they are set to a value of zero. This makes boolean image and is saved under the “Blocker“ folder. A blocker looks like this in Figure A.3.

After making a ring set and blocker both images will appear. Each of them will appear in their respective folders. The two default values for the bottom two boxes can easily exchange scattering images and dark field if the ring center has changed. To change the image you can click on the “change“ button and a pop-up menu of the ring set or blocker folder will appear or manually type the new images. In summary, the yellow panel is used for making the ring set and blocker and you must enter the desired values in the yellow panel before clicking “make ringsets“ or “make blockers“ in the green panel.

A.3 Generating Profiles

Generating profiles is the bulk of this program and is a complicated process using numerous functions to produce the desired profile plot. The advantage of using this program compared to the original method of generating these profile is its ability to generate multiple profiles at the same time. This is due to the fact that many of the XRMS images use the same ring set and blocker. Before generating a profile we need to look at the red panel. Look at Figure A.1 to see the red panel.

You will notice there are three text boxes. In order to generate a profile from the XRMS image three other files must be included the blocker, the ring set, and the dark field. The red panel is to indicate to the user what blocker, ring set, and dark field will be used to generate the profiles.

When you made the ring set and blocker in the yellow panel they will update the text boxes in the red panel automatically. If you did not create ring sets or blockers you can use the “change“ buttons to exchange the default values for the desired ring set or blocker. Make sure that these are the desired value before the generating process starts.

Once the red panel has the right parameters it is time to transform the XRMS images to the profile plots. To begin, click the “Generate“ button in the drop down menu in the green panel. A pop up menu will appear and ask which images you like to generate, this is done by selecting them and then pressing the confirm button. Next a pop-up menu will appear and ask you to select the time scans associated with the images you previously selected. You will notice now that the images and time scans you selected are printed in the table in the blue panel. The blue panel is used simply to display and verify what you selected is what you want to be generated. It is important that the image on the left side is next to the time scan on the right. Having the image and the time scan on the same row indicates that this time scan will normalize that image. It is possible that the uploaded time scan is not associated with the right image. Double check the association in the research notebook. If you select more or less time scans than image files the evaluation box will give you an error and you will have to run the command again. So make sure you select the right amount of files. After verifying the associated time scans with images the program will wait until you click the “continue“ button in the blue panel and the process of generating the profiles continues. The first function the program encounters is automatically making a folder for this sample in the “Analyzed“ folder, the name of the folder is just the image’s name. Here in this folder, the profile plot, the result vectors, and the new scattered image and more will be stored in its own folder. This is helpful to keep track of what images have been organized. Next is grabbing the selected images and summing each of the 2 dimensional plots then subtracting the dark field from each image. This new scattered image is saved in the samples folder under “Analyzed“ It then undergoes an angular integration using the ring set and averaging it with time scan. See Figure A.4

demonstrating how the angular integration works and the time scans.

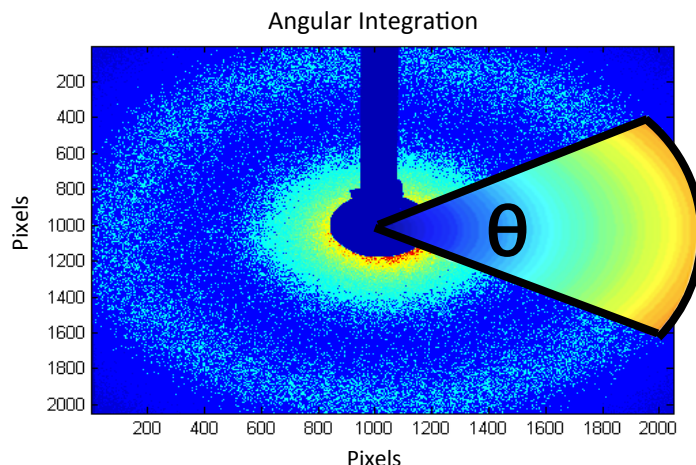


Figure A.4 The image depicts a scattered image being integrated in order to be transformed into a one dimensional intensity profile. You will notice that the blocker and ring set created is apart of the process.

Afterwards it then applies the blocker removing the center of the image. During these procedures a 1- dimensional profile plot is made. A title, axis labels, and legend are given. A quick note is the scattering images were in pixels and now the plots is in terms of the q space which has units of inverse nanometers. Now the plots and the vectors for making the plots are saved for further use in Excel if needed. These vectors are also saved in another folder called "ForComparison".

A.4 Extracting Dichroic Signals

An element of making this program beautiful is its ability to quickly manipulate data so quickly. Apart of the analyzing process is making magnetic ratios and dichroic effect plots. Back in the function of "generate" which made for making profiles, it saves the result vectors in a folder called "ForComparison" this is to our advantage as we can use the files in this folder instead of going through each sample folder to grab the sample vectors. To compare the data we first click on the

“compare“ under the drop down menu in the green panel. A pop-up window of the “ForComparison“ will appear asking you to select the positive results. After clicking “OK“, another pop-up window of the “ForComparison“ will appear asking you to select the negative results. Use the research notebook to see what samples are at positive or negative helicity. You will notice that these samples will fill up the table in the blue table. Verify that the positive sample is next to the corresponding negative file. Then click “Continue“. If you select more or less negative profiles than positive files the evaluation box will give you an error and you will have to run the command again. Make sure you select the right amount of files. The program then runs the function for this command. It will display magnetic ratio plots and dichroic plots and then save both these plots and vectors in both the sample folders. They will not be saved in the “ForComparison“ folder.

In summary, this program is quick and easy to use. Most problems arise when the folder setup process was not done correctly. It is case sensitive so make sure you spell each folder correctly. Other problems arise when use you the program on different computers and the system directory varies. It is common to rewrite the new system directory in the program and is an easy process as you can use the “find“ and “replace all“ command in MATLAB to write the system directory.

Appendix B

Graphs of Model Fits

Many XRMS profiles were made for the charge density function and the charge spin function. This appendix shows the model fits for various samples and their dichroic effect plot. For the charge density model only one sample was model to find the nanoparticle size, interparticle distances and the distribution, see Figure B.1 and B.2. The tables that gathered this information is back in chapter 3. However, because the main purpose of this research project is to find the magnetic ordering of these nanoparticle assemblies more models were made to fit different samples and at various external magnetic field values using the dichroic effect technique. Below in Figure B.3 and B.4 The tables that extracted information from these model fits are in chapter 4 for analyzing purposes.

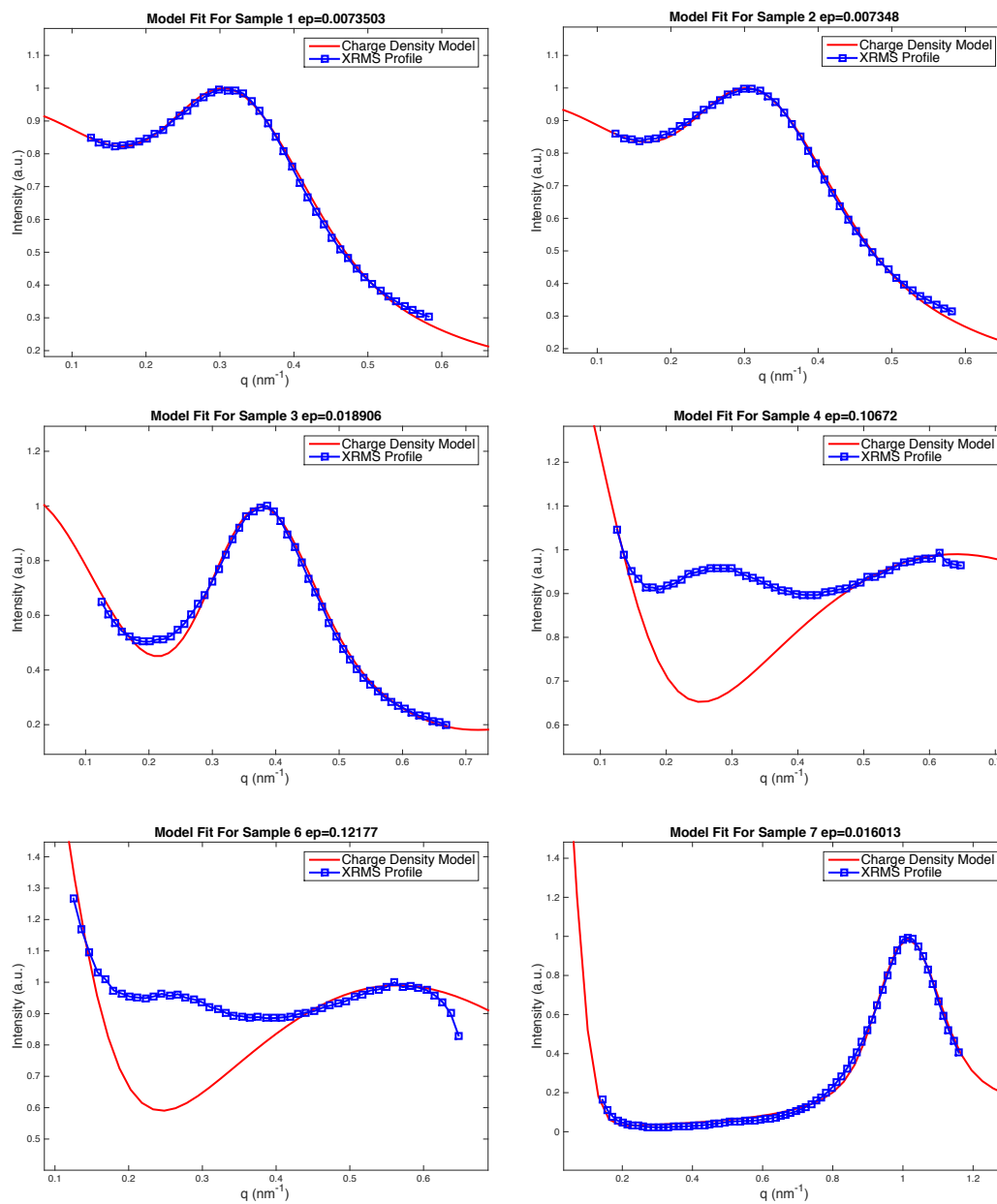


Figure B.1

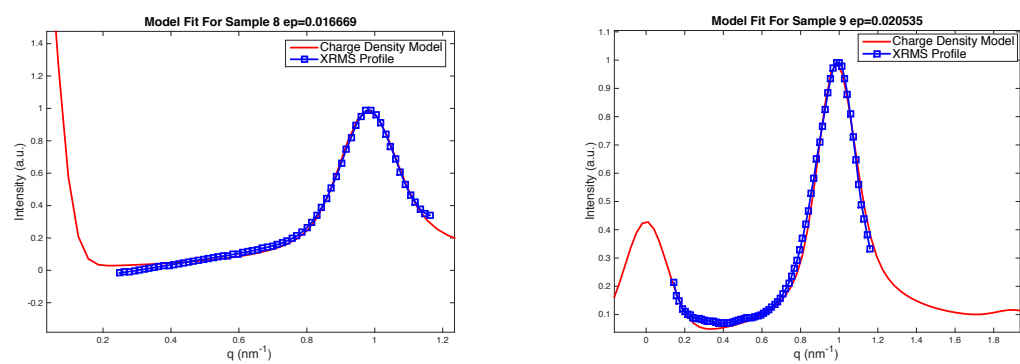


Figure B.2 Models for all of the XRMS profile samples. Sample 5 was excluded due to its poor signal and was unable to be modeled. The models were used to give information about its average nanoparticle size, interparticle distances and distribution. The table that extracted this information is in chapter 3.

Charge Spin Fits Through Magnetization Loop for Sample 2

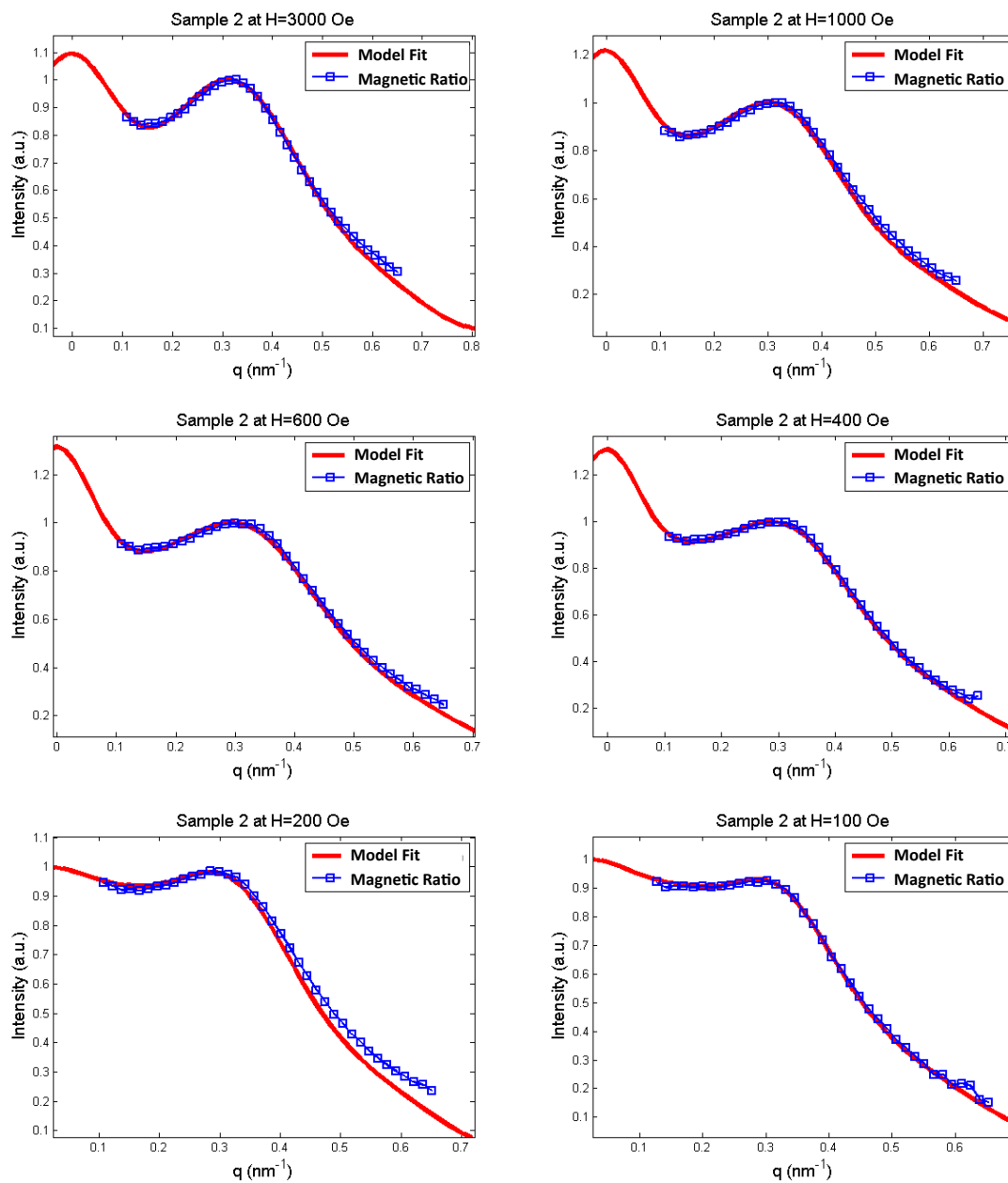


Figure B.3 The charge spin function was fitted on the magnetic ratio plots. The models were performed on sample 2 through a magnetization loop starting at $H=3000$ to $H=-3000$ Oe. Only some of the images are displayed here.

Charge Spin Fits Through Magnetization Loop for Sample 3

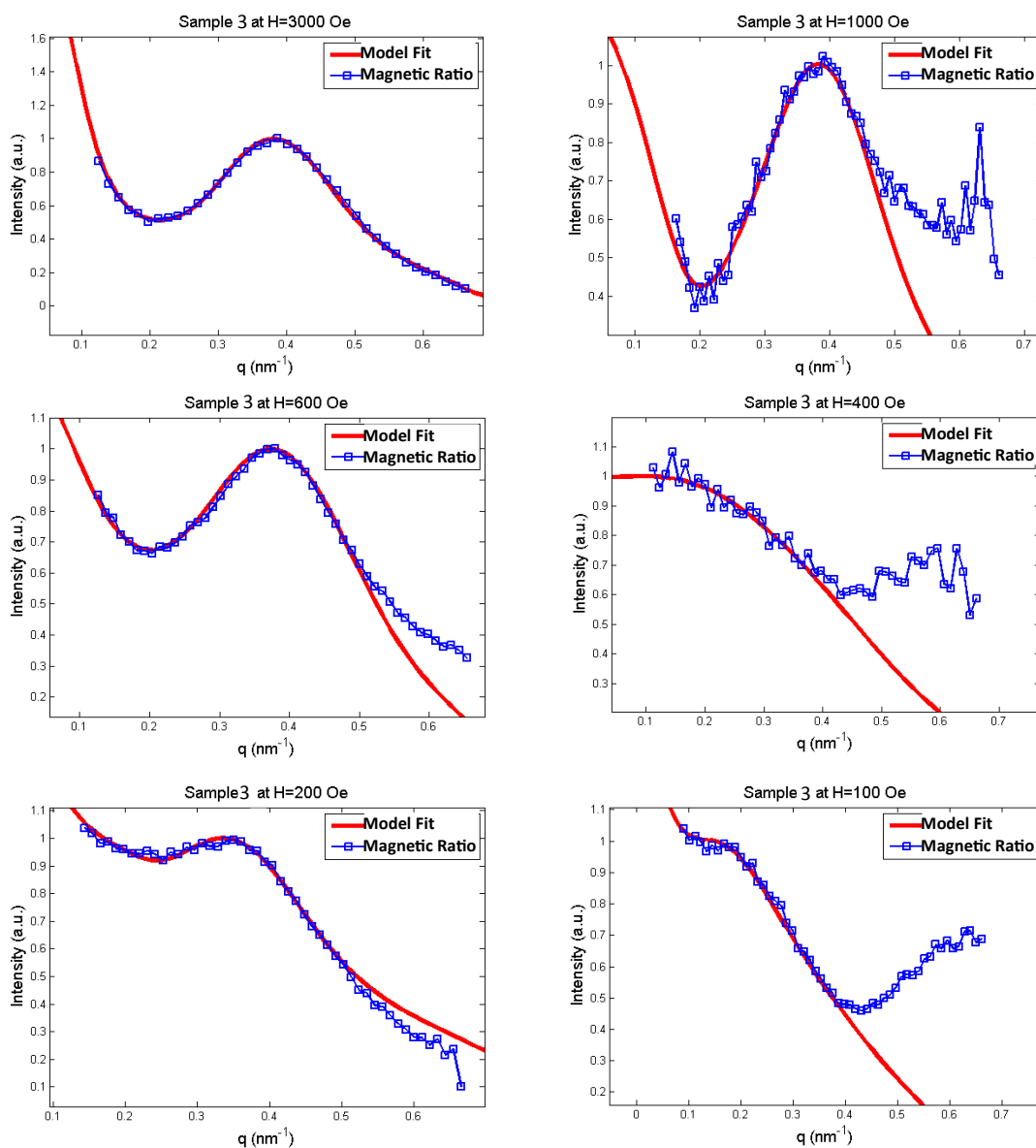


Figure B.4 The charge spin function was fitted on the magnetic ratio plots. The models were performed on sample 3 through a magnetization loop starting at $H=3000$ to $H=-3000$ Oe. Only some of the images are displayed here.

Bibliography

Akbarzadeh, A., Samiei, M., & Davaran, S. 2012, *Nanoscale Research Letters*, 7, 1

Bean, C. P., & Livingston, J. D. 1959, *Journal of Applied Physics*, 30

Cai, Y. P., et al. 2014, *Journal of Applied Physics*, 115

Ito, A., Shinkai, M., Honda, H., & Kobayashi, T. 2005, *Journal of Bioscience and Bioengineering*, 100, 1

Spaldin, N. A. 2010, in *Magnetic Materials*, 2nd edn. (Cambridge University Press), 113–129, [cambridge Books Online](#)

Sun*, S., , & Zeng, H. 2002, *Journal of the American Chemical Society*, 124, 8204, pMID: 12105897

Index

Anti-ferromagnetism, 3, 19, 20, 39

Charge Density Function, 26, 29, 31

Charge Spin Function, 33, 34, 36

Distribution, 16, 24, 37

Ferrimagnetism, 4, 10, 20

Ferromagnetism, 3, 18, 20, 32, 37, 39

Fourier Transform, 25, 32, 33, 36

Inverse Space, 21, 25, 48

Magnetic Ordering, 2, 3, 6, 11, 18, 19, 28, 31

magnetic Spin Function, 29

Magnetite Fe_3O_4 , 1, 3, 10

Magnetization, 17, 33–35

Matlab, 49

Nanoparticles, 2, 20, 22, 29, 33

Paramagnetism, 3

Real Space, 21, 25

Spin, 3, 4

Superparamagnetism, 1, 4, 5, 39

Synchrotron, 1, 5, 35, 41

TEM, 1

Thermal Decomposition, 2

VSM, 34, 35

XAS, 2

XMCD, 2, 5–10, 20

XRMS, 5, 6, 10–12, 14, 16, 17, 20, 21, 25, 26, 28, 29, 31, 41